Chemical Engineering Science 277 (2023) 118802

Contents lists available at ScienceDirect

Chemical Engineering Science

journal homepage: www.elsevier.com/locate/ces

Dynamics of cupcake baking: Coupled multiphase heat and mass transport in a deformable porous material

Kalayarasan Seranthian, Ashim Datta *

Department of Biological and Environmental Engineering, Cornell University, 208 Riley Robb Hall, Ithaca, NY 14853, USA

ARTICLE INFO

Keywords:
Coupled transport and deformation
Evaporation
Phase change
Viscoelasticity
Porous media
Multiphysics modeling

ABSTRACT

This study presents a coupled multiphase porous media transport model with evaporation, large deformation, and material transformation (phase change from starch gelatinization) for cupcake baking in a conventional oven. The governing equations for transport and deformation are energy, mass, and momentum conservation of the solid cupcake batter matrix, water, water vapor, and carbon dioxide produced during baking. They are solved numerically to predict the evolution of the cupcake batter's temperature, moisture, dimensional change, and color during baking. Cupcake-baking experiments are used to validate the model against measured temperature, moisture, color, and cupcake height during baking. The rate of carbon dioxide production, vapor generation, and the cupcake batter's mechanical properties determine the cupcake's final shape. The novelty of the numerical model is the coupling of the massive change in mechanical and thermophysical properties with multiphase transport and expansion due to pressure and moisture loss from shrinkage.

1. Introduction

Cakes are essential bakery products. They generate annual revenue of about 6 billion dollars in the United States. A thorough mechanistic understanding of the cake-baking process is necessary for cake quality, cost reduction, and optimization. Cake baking involves simultaneous heat and mass transfer in a complex mixture of fat-in-water type emulsion accompanied by 100% to 300% size change (Bennion and Bamford, 1997; Pyler and Gorton, 2008; Sumnu and Sahin, 2008). A mechanistic understanding of how this fluid batter rises and sets into a solid, porous structure during the cake baking process is still limited (Sablani et al., 1998; Feyissa et al., 2011; Sakin-Yilmazer et al., 2012; Ureta et al., 2016; Cevoli et al., 2020), even though the baking industry has a history of a few thousand years (Jacob, 2007). Being a traditional process, even now, the process metrics to obtain the desired final shape, size, texture, and color of the cake are primarily based on experience rather than engineering understanding. Mechanistic knowledge is necessary to provide a rational basis for optimization and novel developments in products and processes.

Polymer physics problems, such as polymer gelation, where a liquid polymer solution undergoes a chemical or physical process forming a solid gel, are comparable to cake baking (Tanaka, 2011). Polymer crystallization and polymer crosslinking are temperature-dependent material transformations similar to the material transformation of aqueous cake batter to a solid cake (Rubinstein et al., 2003). Thus, mechanistic knowledge of cupcake baking would extend to these and other engineering applications across disciplines.

1.1. Cake baking process

Fig. 1 shows a schematic of the different mechanisms involved in cake baking. A typical cake-baking process begins with heat transfer into the cake batter. Heat transfer follows vapor generation from the water content in the batter mixture, accompanied by carbon dioxide generation from the baking powder reaction in the batter mixture. Vapor occupies more than 1000 times more volume than water. The vapor and carbon dioxide generation lead to pressure development in the cake batter. This pressure development causes the aqueous, fluid batter (rubbery state) to rise and form a foam-like structure (glassy state) (Guy and Sahi, 2006) while undergoing shrinkage due to moisture loss (Mizukoshi, 1985). The process also accompanies a massive change in mechanical properties due to starch gelatinization in the mixture, which causes the foam-like structure to set thermally (Mizukoshi et al., 1979), making cake baking a very challenging problem to model.

* Corresponding author.
E-mail address: akd1@cornell.edu (A. Datta).

https://doi.org/10.1016/j.ces.2023.118802
Received 20 December 2022; Received in revised form 17 April 2023; Accepted 23 April 2023
Available online 8 May 2023

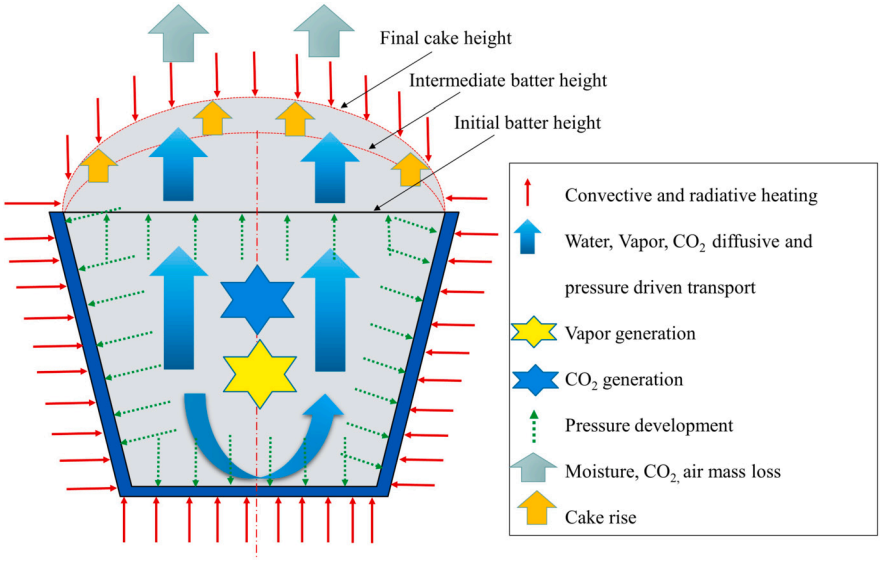

Fig. 1. Schematic showing multimode heat transfer, multiphase mass transport and deformation in a cake baking process.

Table 1
Comparison of this study with previous modeling approaches on cake baking.

Physics modeled	Cake baking: Lostie et al. (2002)	Cake baking: Sakin et al. (2007)	Cake baking: this study
Deformation			
Viscoelasticity	No	No	Yes
Shrinkage due to moisture loss	No	No	Yes
Material transition from rubbery to glassy state	No	No	Yes
Mass transport	Yes	Yes	Yes
Phase change	No	No	Yes
CO_2 generation	No	No	Yes
Heat transport	Yes	Yes	Yes

1.2. Modeling perspective in literature and novelty of current study

Fig. 2 shows a schematic of all the relevant physics involved in a cake-baking. Cake baking involves energy, mass and momentum transport along with significant volumetric change accompanied by a large change in mechanical properties. The process involves a two-way coupling of transport and deformation physics and includes carbon dioxide and vapor generation.

Previous attempts of modeling the cake baking process (Sablani et al., 1998; Feyissa et al., 2011; Sakin-Yilmazer et al., 2012; Cevoli et al., 2020; Lostie et al., 2002; Ureta et al., 2017) were able to accurately describe the heat transfer and part of the mass transfer physics during baking. However, no modeling studies on cake baking include all relevant physics shown in Fig. 2, which explains the lack of mechanistic understanding of cake baking and the need for the current study and its novelty. Table 1 compares the modeling approaches of two relatively advanced works on cake baking: (1) Lostie et al. (2002) and (2) Sakin et al. (2007) with the current study to emphasize this point.

Models that account for transport and large deformation exist for various applications. Zhang and Datta (2006) and Nicolas et al. (2014, 2016) have modeled multiphase transport and large deformation for bread baking, and the mechanistic understanding of bread baking is advanced as compared to cake baking. Cake baking is similar to bread baking with the same relevant physics but with an even greater material transformation from an aqueous batter to a solid foam and a larger volume change. The current study bridges the gap between the mechanistic understanding of bread and cake baking.

1.3. Objectives and overview

The main objectives of this study are as follows: (1) develop a mathematical model for a coupled multiphase heat and mass transport process with large deformation with significant changes in mechanical properties, (2) validate the model with experimentally measured performance metrics of cupcakes (oven rise, color, weight loss, temperatures) for different oven settings during the baking cycle, and (3) identify the critical parameters for the process and perform sensitivity analysis.

2. Model development

2.1. Overall physics

The two significant physical phenomena in cake baking are multiphase transport and large deformation (Fig. 2). This section presents a porous media-based multi-phase, multi-component heat and mass transport framework coupled with large deformations of the viscoelastic solid matrix for cake baking with the major assumptions, governing equations, and initial and boundary conditions. The framework is from well-established conservation equations considering the batter as a porous media through which different phases transport (Datta, 2007).

2.2. Porous media formulation

The first step in the model development is simplifying the porous cake batter by homogenizing it with effective transport properties. Homogenization is necessary for this problem since the dimensions of the pores in the structure are several orders of magnitude smaller than the computational domain, which enables us to make the following significant assumptions (Dhall and Datta, 2011): (1) the mass species (solid, liquid and gas phases) are continuous in the porous medium, (2) there is local thermal equilibrium between the three phases at any spatial location, (3) pressure in the liquid water is the sum of gas pressure and capillary pressure, (4) the solid skeleton is a linear viscoelastic material, (5) solid volume remains constant during any process, and (6) the representative elementary volume over which the physical quantities are averaged will change with pore size and local variations in pore size are ignored.

In addition to the above, we assumed the gas phase to be a binary mixture of water vapor and carbon dioxide with mass fractions ω_v and ω_{CO_2}, respectively. With this simplification, the volumetric concentrations, c_i, in the porous medium relate to the respective relative saturations and mass fractions as follows:

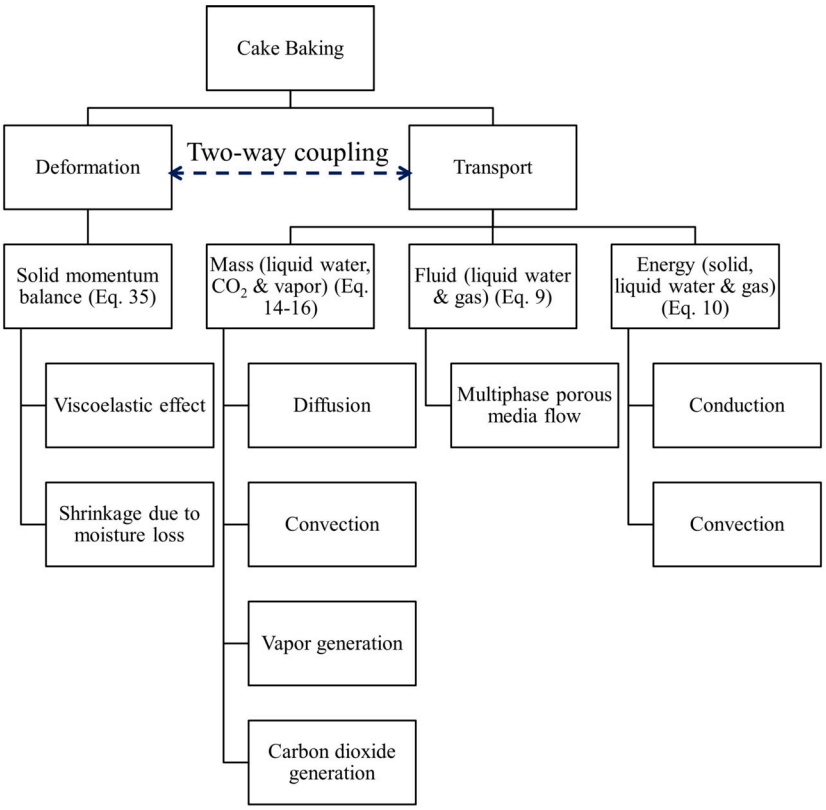

Fig. 2. The different physics involved in a cake baking process. Section 2.3 discusses the equations mentioned.

$$c_w = \rho_w S_w \phi \tag{1}$$

$$c_g = \rho_g S_g \phi \tag{2}$$

$$c_v = \rho_g S_g \phi \omega_v \tag{3}$$

$$c_{CO_2} = \rho_g S_g \phi \omega_{CO_2} \tag{4}$$

$$\omega_{CO_2} = 1 - \omega_v \tag{5}$$

The total porosity, ϕ, is defined as the fraction of volume occupied by fluids (liquid water and gas) in the porous medium as:

$$\phi = \frac{\Delta V_w + \Delta V_g}{\Delta V_s + \Delta V_w + \Delta V_g} \tag{6}$$

and the saturation, S_i, is given as:

$$S_i = \frac{\Delta V_i}{\Delta V_w + \Delta V_g} \quad i = w, g \tag{7}$$

The porous media formulation has allowed the expression of the solid, liquid and gas phases in a continuum. Hence, mathematically, this material continuum is expressed as:

$$\Delta V = \Delta V_s + \Delta V_w + \Delta V_g \tag{8}$$

where s, w and g stand for the solid, water and gas phases, respectively, and V is the total volume of the material.

2.2.1. Darcy's law: momentum conservation

Darcy's law describes the fluid flow in a porous material instead of the Navier-Stokes equations:

$$v_{i,s} = -\frac{k_{in,i} k_{r,i}}{\mu_i} \nabla p_i \quad i = w, g \tag{9}$$

where $v_{i,s}$ is the velocity of phase i relative to the solid phase, $k_{in,i}$, $k_{r,i}$ and p_i are the intrinsic permeability (Sec. 3.2.3), relative permeability and pressure in the phase i, respectively.

2.3. Governing equations

2.3.1. Energy conservation

Governing equations for multiphase heat transport in the porous medium are developed based on the conservation of energy:

$$\rho_{eff} C_{p,eff} \frac{\partial T}{\partial t} + \sum_{i=w,v,CO_2} C_{p,i} (\vec{n}_i \cdot \nabla T) = \nabla \cdot (k_{eff} \nabla T) - \lambda \dot{I} \tag{10}$$

Assuming that the solid, liquid and gas phases are in a continuum and are in thermal equilibrium gives Eqn. (10). The energy equation includes convection of fluid phases, heat conduction and evaporative condensation. Averaging the properties of the individual species that make up the porous medium, weighted by either their mass or volume fractions, gives the effective properties of the porous medium:

$$\rho_{eff} = (1 - \phi)\rho_s + \phi(S_w \rho_w + S_g \rho_g) \tag{11}$$

$$C_{p,eff} = m_s C_{p,s} + m_w C_{p,w} + m_g C_{p,g} \tag{12}$$

$$k_{eff} = (1 - \phi)k_s + \phi(S_w k_w + S_g(\omega_v k_v + \omega_{CO_2} k_{CO_2})) \tag{13}$$

2.3.2. Mass conservation

The four mass species considered in the porous medium are solid, liquid water, water vapor, and carbon dioxide. Water vapor and carbon dioxide are assumed to be ideal gases. Governing equations for multiphase mass transport in a porous medium are developed based on the conservation of mass for liquid water, gas and water vapor:

$$\frac{\partial c_w}{\partial t} + \nabla \cdot \vec{n}_{w,G} = -\dot{I} \tag{14}$$

$$\frac{\partial c_g}{\partial t} + \nabla \cdot \vec{n}_{g,G} = \dot{I} + \dot{R}_{CO_2} \tag{15}$$

$$\frac{\partial c_v}{\partial t} + \nabla \cdot \vec{n}_{v,G} = \dot{I} \tag{16}$$

Equations (14)-(16) solve for the respective concentrations, c_w, c_g and c_v in the porous medium. $\dot{I}$ and $\dot{R}_{CO_2}$ are the rate of evaporation/condensation and carbon dioxide generation, respectively.

Transport fluxes *Liquid water flux:* Gas pressure and capillary pressure drive the liquid water in a porous medium. Gravity is weak in an unsaturated porous material and hence ignored. Therefore, the net pressure acting on the liquid phase is given by:

$$p_w = p_g - p_c \tag{17}$$

where p_g and p_c are the gas and capillary pressures respectively. The negative sign indicates that the capillary pressure is attractive. The liquid water flux, $\vec{n}_{w,s}$, relative to the solid is given by:

$$\vec{n}_{w,s} = -\rho_w \frac{k_{in,w}k_{r,w}}{\mu_i}\nabla p_w \tag{18}$$

$$= -\rho_w \frac{k_{in,w}k_{r,w}}{\mu_w}\nabla p_g + \rho_w \frac{k_{in,w}k_{r,w}}{\mu_w}\nabla p_c \tag{19}$$

$$= \rho_w \vec{v}_{w,s} + \rho_w \frac{k_{in,w}k_{r,w}}{\mu_w}\frac{\partial p_c}{\partial c_w}\nabla c_w \tag{20}$$

$$= \rho_w \vec{v}_{w,s} - D_{w,cap}\nabla c_w \tag{21}$$

where $D_{w,cap}$ is the capillary diffusivity and $\vec{v}_{w,s}$ is substituted from Eq. (9).

Gas flux: The net gas flux relative to the solid, $\vec{n}_{g,s}$, is based on Darcy's law and is given by:

$$\vec{n}_{g,s} = -\rho_g \frac{k_{in,g}k_{r,g}}{\mu_g}\nabla p_g \tag{22}$$

$$= \rho_g \vec{v}_{g,s} \tag{23}$$

Water vapor flux: The driving forces for water vapor transport in the cake are gas pressure and binary molecular diffusion with carbon dioxide. The net vapor flux for the solid, $\vec{n}_{v,s}$, is given by:

$$\vec{n}_{v,s} = -\rho_v \frac{k_{in,g}k_{r,g}}{\mu_g}\nabla p_g - \frac{C^2}{\rho_g} M_v M_{CO_2} D_{bin}\nabla x_v \tag{24}$$

$$\vec{n}_{v,s} = \rho_v \vec{v}_{g,s} - \frac{C^2}{\rho_g} M_v M_{CO_2} D_{bin}\nabla x_v \tag{25}$$

where $\vec{v}_{g,s}$ is substituted from Eq. (9).

The porous material undergoes deformation causing movement of the solid phase. Hence, an additional flux (described in Section 2.3.5) representing solid movement is added to the mass fluxes described above:

$$\vec{n}_{i,G} = \vec{n}_{i,s} + c_i \vec{v}_s \tag{26}$$

Thus, the mass fluxes for the ground frame are given by:

$$\vec{n}_{w,G} = \rho_w \vec{v}_{w,s} - D_{w,cap}\nabla c_w + c_w \vec{v}_s \tag{27}$$

$$\vec{n}_{g,G} = \rho_g \vec{v}_{g,s} + c_g \vec{v}_s \tag{28}$$

$$\vec{n}_{v,G} = \rho_v \vec{v}_{g,s} - \frac{C^2}{\rho_g} M_v M_{CO_2} D_{bin}\nabla x_v + c_v \vec{v}_s \tag{29}$$

2.3.3. Evaporation and condensation

Evaporation of liquid water to vapor causes pressure development in the batter and drives the volumetric change in the baking process. A non-equilibrium formulation (Le et al., 1995; Scarpa and Milano, 2002; Halder et al., 2007) describes the evaporation/condensation distributed spatially in the batter, proportional to the difference between the equilibrium vapor density (also known as saturation vapor density) and the density of vapor in the batter:

$$\dot{I} = K_{evap}(p_{v,eq} - p_v)\frac{S_g \phi}{RT} \tag{30}$$

where $p_v = p_g \omega_v$ is the vapor pressure at any location in the homogenized porous batter, $p_{v,eq}$ the equilibrium vapor pressure corresponding to the temperature and moisture level, and K_{evap} is the empirical evaporation constant. The value of the evaporation constant is large such that any further increase in its value does not affect the solution (Halder et al., 2007). The equilibrium vapor pressure, $p_{v,eq}$, is related to water activity a_w as $p_{v,eq} = p_{sat} a_w$ where p_{sat} is the saturation vapor pressure of pure water (Gulati and Datta, 2016).

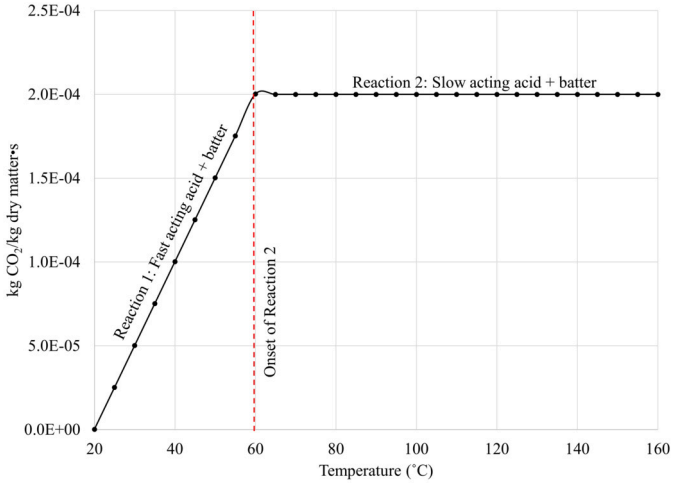

Fig. 3. CO_2 generation from the slow and fast acting acids of baking powder with batter.

2.3.4. Carbon dioxide generation

Double-acting baking powders contain a mixture of carbonate or bicarbonate, fast-acting and slow-acting acids, and a buffer (e.g., dry cornstarch) to prevent premature reactions (Miller, 2016; Godefroidt et al., 2019; Brodie and Godber, 2000). An ideal double-acting baking powder will release 80% of carbon dioxide in the oven (Miller, 2016). Generation of CO_2 is considered to be a zeroth order reaction (Sumnu and Sahin, 2008; Sakin-Yilmazer et al., 2012; Miller, 2016):

$$\dot{R}_{CO_2} = \begin{cases} \rho_s(1-\phi)(5\times10^{-4}(T-273.15) - 9.98\times10^{-5}), & T \le 60\,^{\circ}\mathrm{C} \\ \rho_s(1-\phi)(5\times10^{-4}(333.15-273.15) - 9.98\times10^{-5}), & T > 60\,^{\circ}\mathrm{C} \end{cases} \tag{31}$$

where $\dot{R}_{CO_2}$ is the mass generation rate of CO_2 in the volumetric basis of the cake batter. The units of $\dot{R}_{CO_2}$ are in $\mathrm{kgCO_2/s/volume\ of\ batter}$. Fig. 3 shows the temperature dependency of the mass generation rate of CO_2 in the mass basis of baking powder.

We do not know the exact carbon dioxide generation model for the commercial baking powder used in this study. But, this model of CO_2 generation is consistent with experimental observation (Daniels and Fisher, 1976; Book et al., 2015). The onset of the reaction from the slow-acting acid in the double-acting baking powder is assumed to be at 60 °C, consistent with the experimental observations (Book et al., 2015). The slope of the reaction rate for the carbon dioxide generation rate from the fast-acting acid is chosen such that the total amount of CO_2 generated is approximate to that reported for a typical baking process, which is 15 to 30% of the weight of baking powder (Foot, 1906).

2.3.5. Linear momentum conservation

The linear momentum conservation equation for the porous matrix in a stress-free state is given by:

$$\overline{\nabla}\cdot\overline{\sigma}_{total} = 0 \tag{32}$$

where,

$$\overline{\sigma}_{total} = \overline{\sigma}_{eff} - p_f \mathbf{I} \tag{33}$$

Thus, the divergence of the effective stress in the solid porous matrix is equal to the gradient of fluid pressure generated during baking, as given by:

$$\overline{\nabla} \cdot \overline{\sigma}_{eff} = \overline{\nabla} p_f \tag{34}$$

In cake baking, the contributions to the total stress from the fluid phase are primarily due to gas (vapor and carbon dioxide) generation. Thus, the equation for the conservation of linear momentum in the cake batter is:

$$\overline{\nabla} \cdot \overline{\sigma}_{eff} = \overline{\nabla} p_g \tag{35}$$

Equation (35) solves for the deformation of the porous cake batter during the baking process. Since the porous cake batter undergoes large deformation, the Lagrangian formulation defines the effective stress as:

$$\overline{\sigma}_{eff} = J^{-1} \mathbf{F} \cdot \mathbf{S} \cdot \mathbf{F^T} \tag{36}$$

where J, $\mathbf{F}$ and $\mathbf{S}$ are the Jacobian, deformation gradient tensor and second Piola-Kirchhoff (PK2) stress tensor, respectively. The Jacobian, J, is the volume change ratio of the material and is calculated by computing the determinant of the deformation gradient tensor, $\mathbf{F}$. The deformation gradient tensor is related to the Green-Lagrange strain tensor, $\mathbf{E}$, by:

$$\mathbf{E} = \frac{1}{2}\mathbf{F^T F} - \mathbf{I} \tag{37}$$

The total strain expressed in terms of the total material displacement, u,

$$\mathbf{E} = \frac{1}{2}\left[(\overline{\nabla} \cdot \overline{u}) + (\overline{\nabla} \cdot \overline{u})^T + (\overline{\nabla} \cdot \overline{u})(\overline{\nabla} \cdot \overline{u})^T\right] \tag{38}$$

the solid velocity of the deforming porous matrix is given by:

$$\overline{v_s} = \frac{d\overline{u}}{dt} \tag{39}$$

2.3.5.1. Multiplicative split of the deformation gradient tensor The deformation mechanics of the porous cake matrix during baking is oven rise due to gas pressure and shrinkage during drying due to moisture changes. Hence, the deformation gradient, F, of the porous cake matrix that maps the displacements in the reference configuration to the deformed configuration is a multiplicative split of the elastic and moisture effects causing the total material deformation (Dhall and Datta, 2011; Vujošević and Lubarda, 2002):

$$\mathbf{F} = \mathbf{F_{el}} \mathbf{F_M} \tag{40}$$

2.3.6. Solid mechanics formulation: shrinkage due to moisture loss

The contribution to total volume changes of the porous cake matrix due to moisture loss relates to changes in the liquid water content. Hence, the volume change due to moisture loss, J_M, is calculated by associating it to the volume fraction of the liquid water phase (Dhall and Datta, 2011; Aregawi et al., 2013):

$$J_M = \frac{1 - \phi_{w,0}}{1 - \phi_w} \tag{41}$$

$$\mathbf{F_M} = J_M \mathbf{I} \tag{42}$$

2.3.7. Solid mechanics formulation: constitutive law

Cake batters exhibit both viscous and elastic characteristics when undergoing deformation (Sumnu and Sahin, 2008; Mizukoshi, 1985; Mizukoshi et al., 1979, 1980). They also undergo a large change in mechanical properties due to change in water content (Sumnu and Sahin, 2008) and material transformation (Mizukoshi, 1985). The properties have a strong temperature dependence. Based on this, linear viscoelasticity accounts for the large material deformation during the baking process. This study uses the Kelvin-Voigt linear model comprising a parallel arrangement of a purely viscous damper of viscosity, η, and a purely elastic spring of modulus of elasticity, E, (Epaarachchi, 2011; Hajikarimi and Nejad, 2021). The constitutive relation is expressed as a linear first-order differential equation:

$$\sigma(t) = E\varepsilon + \eta\dot{\varepsilon} \tag{43}$$

where ε and $\dot{\varepsilon}$ are the elastic strain and strain rate, respectively. Thus, for instantaneous stress, σ_0, the elastic strain in the viscoelastic material, is given by:

$$\varepsilon(t) = \frac{\sigma_0}{E}(1 - e^{-t/\tau}) \tag{44}$$

where $\tau = \eta/E$ is the relaxation time. The temperature dependence of modulus of elasticity ($E(T)$) and relaxation time ($\tau(T)$) captures the viscoelastic behavior of the batter as a function of the material state throughout the baking process.

2.3.8. Pore formation

The oven rise during baking is caused by pressure development in the batter due to vapor and carbon dioxide generation. Individually, the solid and the fluid phases are incompressible, but the deformation during baking changes local porosity. Thus, at any time, t, ϕ in the deforming porous matrix can be obtained by conserving the volume of the solid phase as:

$$(1 - \phi(t))\Delta V = (1 - \phi_0)\Delta V_0 \tag{45}$$

$$\phi(t) = 1 - \frac{(1 - \phi_0)}{J} \tag{46}$$

2.4. Color model

The color of a cake is a critical quality parameter. The formation of yellow-gold color on the surface of cakes, often called browning, is due to the Maillard reaction and caramelization of sugars (Zanoni et al., 1995; Fennema, 1996; Martins et al., 2000), and is influenced by several factors, including temperature, pH, moisture content, and the presence of salt, acid, and other enzymatic agents. Color difference, ΔE, between the raw batter and the baked cupcake samples quantifies surface browning according to the following equation:

$$\Delta E = \sqrt{(L_0^* - L^*)^2 + (a_0^* - a^*)^2 + (b_0^* - b^*)^2} \tag{47}$$

where L^*, a^*, and b^* are the lightness, redness and yellowness measurements of color, respectively. (ΔE) is the Browning Index of the sample.

Browning is assumed to be only temperature dependent and follow first-order kinetics (Zanoni et al., 1995; Purlis and Salvadori, 2009):

$$\frac{d(\Delta E)}{dt} = -k_{br}(\Delta E) \tag{48}$$

$$k_{br} = k_0 e^{-A/T(t)} \tag{49}$$

where k_0 and A are fitting parameters and $T(t)$ is the surface temperature evolution during baking, computed from the mathematical model.

3. Model parameters

3.1. Boundary conditions

The boundary conditions for the governing equations discussed in Sec. 2.3 and as shown in Fig. 4 are described below.

3.1.1. Heat transfer

The boundary conditions in the computational model for Eq. (10), which solve for the internal temperatures in the porous cake batter, are described here. As shown in Fig. 4, boundary 1 is axisymmetric. Hence, the boundary condition here for the energy equation is given by:

$$\left.\frac{dT}{dr}\right|_{r=0} = 0 \tag{50}$$

Convective and radiative heat transfer at the boundaries 2, 3 and 4 are the driving forces for cake baking. The bottom and lateral surfaces of

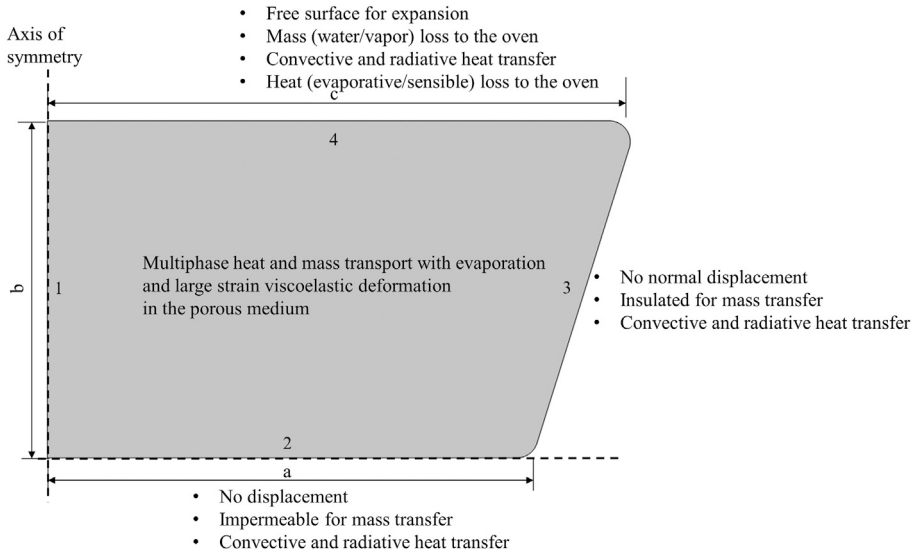

Fig. 4. Schematic showing the cupcake geometry and boundary conditions for the coupled solid mechanics - multiphase transport model.

the cupcake receive the same heat as the cupcake sits on a metal tray, i.e., the resistance of the metal tray is ignored. Hence, the boundary condition on boundaries 2 and 3 is given by:

$$q|_{2,3} = h_c(T_{a,bottom} - T) + h_r(T_{wa,bottom} - T) \tag{51}$$

where $T_{a,bottom}$ is the measured air temperature just below the cupcake tray, $T_{wa,bottom}$ is the surface temperature of the oven bottom, and h_c and h_r are the heat transfer coefficients for convective and radiative heat exchange, respectively. The boundary condition for radiative heat exchange, $h_r(T_{wa,top} - T)$, is an approximation of $\sigma F_{wa-surf}(T^4_{wa,top} - T^4)$ (Incropera and DeWitt, 1985), where σ is the Stefan-Boltzmann constant, and $F_{wa-surf}$ is the view factor between the wall and cake surface. The boundary condition for boundary 4 of the cupcake is:

$$q|_4 = h_c(T_{a,top} - T) + h_r(T_{wa,top} - T) - \lambda\, \vec{n}_{w,s}|_4 - \sum_{i=w,v,CO_2} (\vec{n}_{i,G}|_4) C_{p,v} T \cdot \vec{N}\Big|_4 \tag{52}$$

where $T_{a,top}$ is the air temperature just above the cupcake in the tray, $T_{wa,top}$ is the surface temperature of the top oven wall, and h_c and h_r are the heat transfer coefficients for convective and radiative heat transfers, respectively. In Eq. (52), the third and the fourth terms are the evaporative and sensible heat loss from the cupcake surface to the oven, respectively. $\vec{N}\Big|_4$ is the unit surface normal. $T_{a,bottom}$, $T_{wa,bottom}$, $T_{a,top}$ and $T_{wa,top}$ are experimentally measured as discussed in Section 5.2.

3.1.2. Mass transfer

The boundary conditions for the mass transfer equations at the axisymmetric boundary 1 and boundaries 2 and 3, representing the bottom and lateral surfaces of the cake touching the metal tray, are set to zero mass flux. Boundary 4 represents the top surface of the cupcake where a convective mass transfer boundary condition is used. Since the cupcake geometry undergoes deformation causing movement of the solid phase, an additional flux defining solid movement is added:

$$\vec{n}_{w,G}|_4 = h_m S_w \phi \rho_{g,4} \omega_{v,4} + c_w \vec{v}_s \tag{53}$$

Similar to liquid water, the water vapor in the batter at the top surface is convected away:

$$\vec{n}_{v,G}|_4 = h_m S_g \phi \rho_{g,4} \omega_{v,4} + c_w \vec{v}_s \tag{54}$$

The cupcake is baked at ambient pressure conditions leading to the boundary condition for the gas mass transfer equation (Eq. (15)) at the top surface as:

$$p|_4 = p|_{amb} \tag{55}$$

3.1.3. Solid mechanics

The boundary conditions in the computational model for Eq. (35), which solve for the volumetric deformation ($\vec{v}_s$) of the porous cake batter, are described here. Displacements normal to the axis of symmetry (boundary 1) and the lateral surface (boundary 3) are set to zero. The bottom surface (boundary 2) is fixed, while the top surface (boundary 4) is unconstrained and free to deform.

3.2. Input parameters

Table 2 summarizes the input parameters used in simulating the model equations. Details of some of the critical parameters are discussed below.

3.2.1. Diffusion coefficients

Diffusivity of water through the porous media of the batter is temperature and moisture-dependent (van der Lijn, 1976), and the binary diffusivity for water vapor in the air is pressure and temperature-dependent (Moldrup et al., 2005):

$$D_{w,cap} = 1.35 \times 10^{-8} \times exp\left[\frac{-21.61(548 - T)(1.194 + 3.68M)}{T(1 + 18.98M)}\right] \tag{56}$$

$$D_{bin} = 1.6 \times 10^{-5}(S_g \phi)^{4/3} \tag{57}$$

3.2.2. Thermal properties

The specific heat capacity of liquid water, water vapor, and air are temperature dependent (Choi and Okos, 1986; Lewis, 1990):

$$C_{p,w} = 4176.2 - 0.0909(T - 273) + 5.4731 \times 10^{-3}(T - 273)^2 \tag{58}$$

$$C_{p,v} = 1790 + 0.107(T - 273) + 5.856 \times 10^{-4}(T - 273)^2 - 1.997 \times 10^{-7}(T - 273)^3 \tag{59}$$

$$C_{p,a} = 1004.828 - 0.01185(T - 273) + 4.3 \times 10^{-4}(T - 273)^2 \tag{60}$$

as is the thermal conductivity of water (Choi and Okos, 1986):

$$k_w = 0.57109 + 0.0017625T - 6.7306 \times 10^{-6}T^2 \tag{61}$$

3.2.3. Permeability

The intrinsic permeability value that characterizes the ease with which the cake material allows a fluid to pass through it depends on the material state. It undergoes a large change during baking and is

Table 2
Input parameters used in the simulation for cake baking.

Parameter	Value	Units	Source
Geometry			
Bottom radius, a	23	mm	Experiment
Axisymmetric axis, b	16	mm	Experiment
Top radius, c	28	mm	Experiment
Density			
Water, ρ_w	998	kg/m^3	McCabe et al. (1993)
Vapor, ρ_v	Ideal gas	kg/m^3	
Air, ρ_g	Ideal gas	kg/m^3	
Solid, ρ_s	$\frac{\rho_{0,eff}-\phi_0\rho_f}{1-\phi_0}$	kg/m^3	
Specific heat capacity			
Water, $C_{p,w}$	Eq. (58)	J/kg K	Lewis (1990)
Vapor, $C_{p,v}$	Eq. (59)	J/kg K	Lewis (1990)
Air, $C_{p,a}$	Eq. (60)	J/kg K	Choi and Okos (1986)
Solid, C_{ps}	2200	J/kg K	Lostie et al. (2002)
Thermal conductivity			
Water, k_w	Eq. (61)	W/m K	Choi and Okos (1986)
Vapor, k_v	0.026	W/m K	Choi and Okos (1986)
Air, k_a	0.026	W/m K	Choi and Okos (1986)
Solid, k_s	0.12	W/m K	Lostie et al. (2004)
Intrinsic permeability			
Water, $k_{in,w}$	Fig. 5	m^2	Warning et al. (2014)
Air and vapor, $k_{in,g}$	Eq. (62)	m^2	Tanikawa and Shimamoto (2009)
Relative permeability			
Water, $k_{r,w}$	Eq. (63)		Bear (1988)
Air and vapor, $k_{r,g}$	Eq. (64)		Bear (1988)
Porosity factor, $f(\phi)$	Eq. (65)		Bear (1988)
Capillary diffusivity			
Water, $D_{w,cap}$	Eq. (56)	m^2/s	van der Lijn (1976)
Vapor diffusivity			
In air, D_{bin}	Eq. (57)	m^2/s	Moldrup et al. (2005)
Viscosity			
Water, μ_w	0.988×10^{-3}	Pa.s	McCabe et al. (1993)
Air and vapor, μ_g	1.8×10^{-5}	Pa.s	McCabe et al. (1993)
Convective heat transfer coefficient, h_t	25	W/m^2 K	Sakin et al. (2007, 2009)
Radiative heat transfer coefficient, h_r	6	W/m^2 K	Sakin et al. (2007, 2009)
Mass transfer coefficient, h_m	0.01	m/s	
Latent heat of vaporization, λ	2.26×10^6	J/kg	Schwartzberg et al. (1995)
Equilibrium vapor pressure, $p_{v,eq}$	$a_w \times p_{v,sat}$	kPa	Basu et al. (2006); Andrade et al. (2011)
Saturation vapor pressure, $p_{v,sat}$	Eq. (67)	kPa	
Water activity, a_w	Eq. (68)		
Elastic modulus, $E(T)$	Fig. 7a	Pa	
Relaxation time, $\tau(T)$	Fig. 7b	s	
Initial conditions			
Porosity, ϕ_0	0.5	-	Lostie et al. (2002)
Pressure, P_0	101,325	Pa	
Water concentration, $c_{w,0}$	$\rho_w S_{w,0}\phi_0$	kg/m^3	This study
Water saturation, $S_{w,0}$	$\frac{M_0(1-\phi_0)\rho_s}{\phi_0\rho_w}$	-	This study
Moisture, M_0	0.44	-	This study
Vapor mass fraction, $\omega_{v,0}$	0.01204	-	This study
Temperature, T_0	25	°C	This study
Batter density, $\rho_{0,eff}$	856.26	kg/m^3	This study

different for the batter and the cake. The temperature-dependent intrinsic permeability of the material for liquid water used in the study is shown in Fig. 5. A constant permeability value of 1×10^{-10} m^2 is used to characterize the fluid batter, which decreases to 5×10^{-13} m^2 after starch gelatinization (Lostie et al., 2004). The permeability value used to characterize the sponge cake after starch gelatinization is a measured value for sponge cake crumbs by Lostie et al. (2004).

The intrinsic permeability values of gas are dependent on the water permeability and gas pressure and are given by Tanikawa and Shimamoto (2009):

$$k_{in,g} = k_{in,w}\left(1+\frac{0.15k_{in,w}^{-0.37}}{p}\right) \tag{62}$$

The relative permeability values of water and gas are dependent on the water saturation and are given by Bear (1988):

$$k_{r,w} = \begin{cases} f(\phi)((S_w-0.09)/0.91)^3, S_w > 0.09 \\ 0, S_w < 0.09 \end{cases} \tag{63}$$

$$k_{r,g} = \begin{cases} f(\phi)(1-1.1S_w), S_w < 0.91 \\ 0, S_w > 0.91 \end{cases} \tag{64}$$

where $f(\phi)$ is the porosity factor. During baking, the cake batter undergoes significant volume change resulting in a substantial increase in the material's porosity, leading to increased gas and liquid permeability. Kozney-Carman's porosity factor quantifies this change (Bear, 1988):

$$f(\phi) = \left(\frac{\phi}{\phi_0}\right)^3\left(\frac{1-\phi_0}{1-\phi}\right)^2 \tag{65}$$

3.2.4. Water activity

Water activity, a_w, is the partial vapor pressure of water in a substance divided by the standard state vapor pressure (saturation vapor pressure) of water under distilled conditions.

$$a_w = \frac{p_{v,eq}}{p_{v,sat}} \tag{66}$$

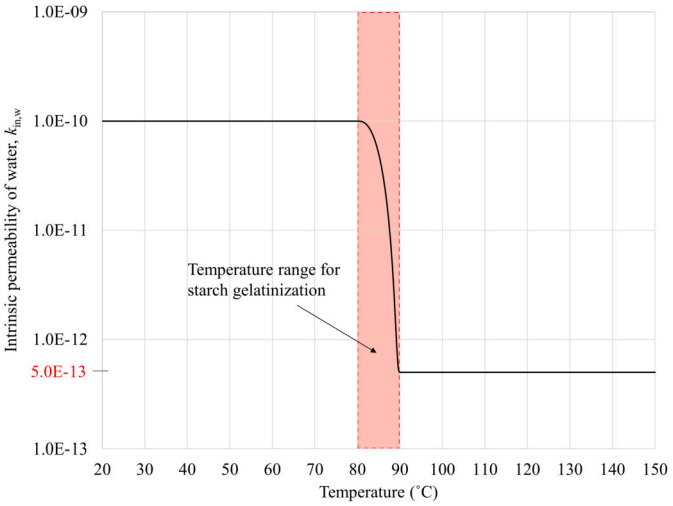

Fig. 5. Intrinsic permeability evolution with temperature based on literature data and assumed variation during the starch gelatinization, which begins at 80 °C and ends at 90 °C (see also Fig. 7).

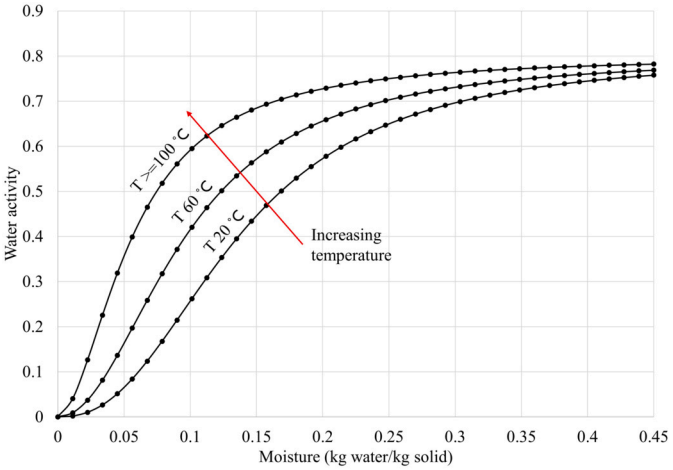

Fig. 6. Water activity evolution with temperature and moisture.

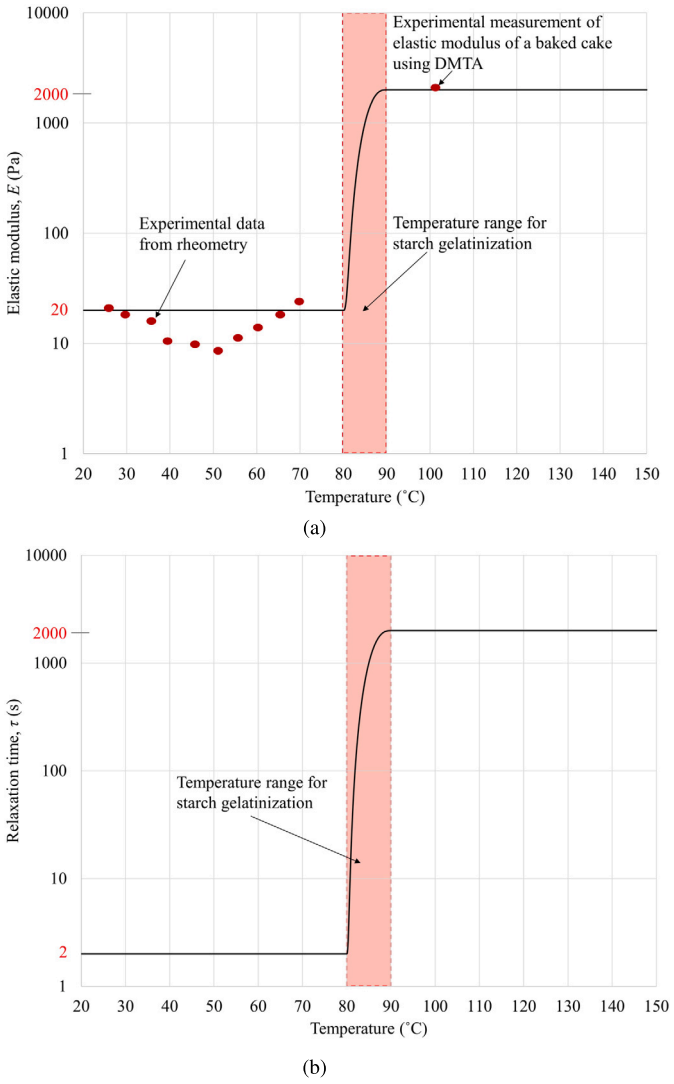

Fig. 7. (a) Elastic modulus and (b) relaxation time evolution with temperature.

where the saturation vapor pressure (in mg of Hg) as a function of temperature given by the Antoine Equation (Antoine, 1888) is:

$$\begin{aligned}\log_{10}(p_{v,sat}) &= 8.07131 - \left[\frac{1730.63}{233.426+(T-273.15)}\right], \; T \le 373.15 \text{ K} \\ \log_{10}(p_{v,sat}) &= 8.14019 - \left[\frac{1810.94}{244.485+(T-273.15)}\right], \; T > 373.15 \text{ K}\end{aligned} \tag{67}$$

Water activity and water content are measured at various operating temperatures to generate desorption isotherms. However, baking involves simultaneous temperature and moisture changes with substantial volume expansion. Hence, the water activity data in the batter during such a complex process are unavailable for the moisture and temperature range. The study uses Oswin's empirical relation to model water activity and its temperature and moisture dependence (see Fig. 6) (Basu et al., 2006; Andrade et al., 2011):

$$\begin{aligned}100M &= A\left(\frac{a_w}{0.65-a_w}\right)^B \\ \text{with} &\begin{cases} A = 15.64 - 0.1(T-273.15)) \\ B = 0.38 + 1.69\times10^{-3}(T-273.15) \end{cases}, \; T < 373.15 \text{ K} \\ 100M &= A\left(\frac{a_w}{0.65-a_w}\right)^B \\ \text{with} &\begin{cases} A = 15.64 - 0.1(373.15-273.15)) \\ B = 0.38 + 1.69\times10^{-3}(373.15-273.15) \end{cases}, \; T \ge 373.15 \text{ K}\end{aligned} \tag{68}$$

The empirical parameters A and B in the water activity relation used are computed by fitting the Oswin model to the desorption isotherm for sponge cake batter (Lostie et al., 2002) for the temperature range 20 °C to 100 °C. The relation does not account for temperature dependency at temperatures higher than 100 °C as there is no significant change to water activities at higher temperatures as described by Bassal et al. (1993). A sensitivity analysis of the water activity relation used was carried out later.

3.2.5. *Material modulus and relaxation times*

The cake batter is viscoelastic, the mechanical properties of which are functions of temperature. The viscoelastic model requires the elastic modulus and relaxation time as functions of temperature. These properties undergo a large change as they depend on the material state. Fig. 7a shows the temperature-dependent elastic modulus used in the study. A constant elastic modulus value of 20 Pa characterizes the elastic nature of the aqueous batter (rubbery state), which increases to 2000 Pa at the starch gelatinization temperature to thermally set to the foam-like structure (glassy state) (Guy and Sahi, 2006). This study ignores the batter's thixotropic behavior (decreased elastic modulus with increased temperature). The experimental data from rheometry and Dynamic Mechanical Thermal Analysis (DMTA) guided the elastic modulus values. The relaxation times undergo a similar transformation to the elastic modulus, as shown in Fig. 7b. A short nominal relaxation time (2 s) is considered

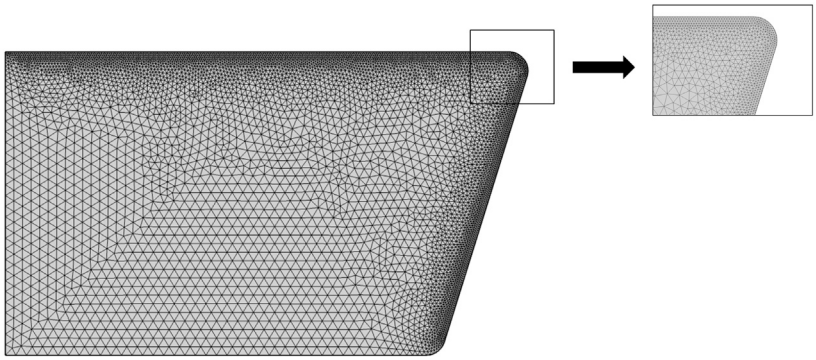

Fig. 8. Meshed geometry with triangular mesh elements. Mesh density is higher close to the top and lateral boundaries to help convergence.

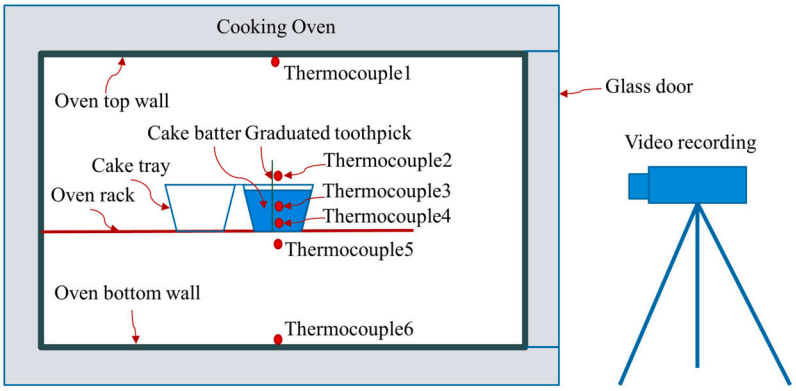

Fig. 9. Experimental setup for cake baking.

for the liquid batter (Zhang and Datta, 2006; Nicolas et al., 2016) followed by an increase (2000 s) with starch gelatinization between 80 °C to 90 °C (Godefroidt et al., 2019) characterizing the formation of set product.

4. Solution methodology: geometry, mesh and implementation

A transient 2D axisymmetric model (see Fig. 4) was used to study the multiphase transport and oven rise in the cupcake during baking by solving a system of coupled equations for solid momentum balance, mass, and energy conservation in a porous media framework. A triangular mesh (see Fig. 8) consisting of 11,374 elements with more elements along the lateral and top boundaries of the 2D geometry was used to help convergence.

COMSOL Multiphysics 5.5 (Comsol Inc., Burlington, MA) was used to solve the governing equations (discussed in Section 2.3) in the computational model. Deformation of the porous batter was computed by solving solid momentum balance in the Lagrange frame of reference using the Structural Mechanics module. The concentrations of liquid water, gas, and water vapor were computed by solving mass conservation equations in the Eulerian frame using the Transport Of Dilute Species, Darcy's Law and Transport of Concentrated Species modules, respectively. The solid momentum balance, the mass, and energy conservation equations were coupled as explained in Section 2.3.

For all the variables, linear shape functions were used. Due to the sheer size of the problem owing to the length of the baking process and the complex coupling of governing equations together with non-linear material properties, the direct solver PARDISO was used. Variable time stepping with a maximum time step size of 0.1 s was used to solve the problem. The simulation of 25 minutes of baking took approximately 42 h of CPU time on a 2.3 GHz 72-core Intel Xeon Workstation with 192 GB RAM. Only 48 cores were used, as any further increase in the number of cores did not speed up the simulation more.

The parameter estimation of the fit parameters in Eq. (48) was done by minimizing the sum of squared differences between the experimental and predicted color development at the top surface of the cupcake sample using the lsqnonlin solver for non-linear least squares in MATLAB (R2017a, The Mathworks Inc., MA, USA). In Eqs. (48)-(49), the experimental data set for color was the average measured surface browning indices (ΔE values) from cupcakes baked with the oven set at 176.7 °C (350 °F). The temperatures used for the estimation were the model-computed average cupcake surface temperature for baking at the oven setting of 176.7 °C (350 °F). The kinetic model parameters (k_0 and A) estimated this way were used to validate the experimental data for cupcakes baked at a different temperature, i.e., oven setting of 190.6 °C (375 °F).

5. Experimental methodology

5.1. Baking experiments

Cake baking experiments were carried out in a Whirlpool 8.7×10^{-2} m^3 (3.1 cubic ft) capacity single wall conventional (no fan) gas oven (Model: Minerva series). The oven comes with an inbuilt temperature management system. The fresh cake batter was prepared for each experiment after the oven was preheated to 176.7 °C (350 °F) to obtain uniform oven baking conditions. The cake batter was prepared by thoroughly mixing flour, sugar, shortening, eggs, milk, salt, and baking powder. The shortening and sugar were mixed first in a stand mixer (KitchenAid, Artisan Series 5) at speed 4 for 2 minutes. Presifted flour, baking powder, milk, and eggs were added to the stand mixer and beaten at speed 4 for 1 minute to ensure a uniform mixture. Twenty-eight grams of batter were then transferred to a parchment paper lined, Teflon-coated cupcake baking tray and baked in the setup shown in Fig. 9 for 25 minutes. The experiments were replicated three times to estimate variability between experiments. This variability is plotted as error bars on the averaged quantities for all measurements from the

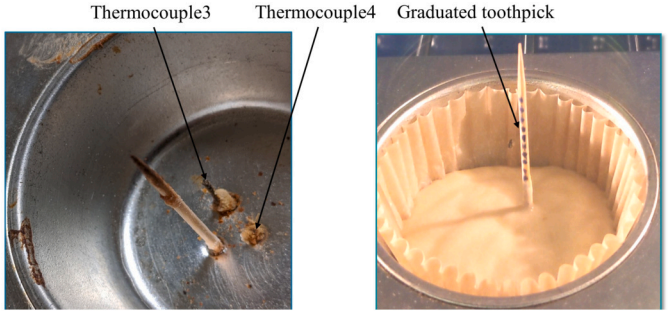

Fig. 10. Experimental setup for internal temperature and oven rise measurement. The cupcake thermocouples are 2 mm and 11 mm from the bottom surface of the cupcake tray (left figure). The toothpick and the thermocouples are fixed at 2 mm radially from the center of the tray. The toothpick was graduated every 1 mm.

experiments. Only one cupcake was baked per experiment. The input parameters for the model, such as the initial moisture content (mass of water/mass of dry matter) and batter density (mass/volume), were measured. The experiments were repeated with the oven preheated to 190.6 °C (375 °F).

5.2. Air temperature and wall temperature measurement

The oven was fitted with four thermocouples to measure the air and wall temperatures inside the oven, as shown in Fig. 9. Thermocouple2, measuring the air temperature, $T_{a,top}$, above the cupcake tray, was fitted 10 mm above the cupcake tray. Thermocouple5, measuring the air temperature, $T_{a,bottom}$, below the cupcake tray, was fitted 10 mm below the cupcake tray. Thermocouple1 and thermocouple6, measuring the top and bottom wall temperatures, $T_{wa,top}$ and $T_{wa,bottom}$, were fitted at the center of the top and bottom walls of the oven cavity, respectively. The thermocouples used were Omega Engineering Inc. K-type (accurate to +/-2.2 °C or +/-0.75%, whichever is greater). Fig. 11a and Fig. 11b show the temperature measurements from these thermocouples recorded throughout the baking process. The air temperatures inside the oven exhibited significant variations between baking.

5.3. Internal temperature and oven rise measurement

The cupcake baking tray was fitted with two thermocouples - one at the point close to the bottom surface (2 mm from the bottom) and another at a point close to the center (11 mm from the bottom) of the cupcake batter, as shown in Fig. 10. The thermocouples used were K-type, and the temperature measurements were recorded throughout the baking process. The baking tray also had a calibrated toothpick fitted at 2 mm from the center, as shown in Fig. 10. The oven-rise evolution throughout the baking process was recorded by monitoring the cupcake height using the graduated toothpick. The thermocouples and the toothpick did not move during baking.

5.4. Moisture loss and color measurement

The weight loss during baking was taken as a measure of moisture loss. Moisture loss measurements at different baking times were carried out by weighing the cupcakes at various times during the baking process. The cupcakes were removed from the baking tray and weighed on a digital kitchen scale (accurate to +/-0.1 g). Each time moisture loss was measured, the cupcake was discarded, and the experiment was repeated for the next time increment with a fresh batter. Moisture loss measurements were made at 10, 13, 16, 19, 22, and 25 minutes.

Color measurements were done using a VeyKolor colorimeter (accurate to +/-0.08 ΔE). After being weighed, the cupcakes were transferred to a wire tray on a bench top under white light. The white light

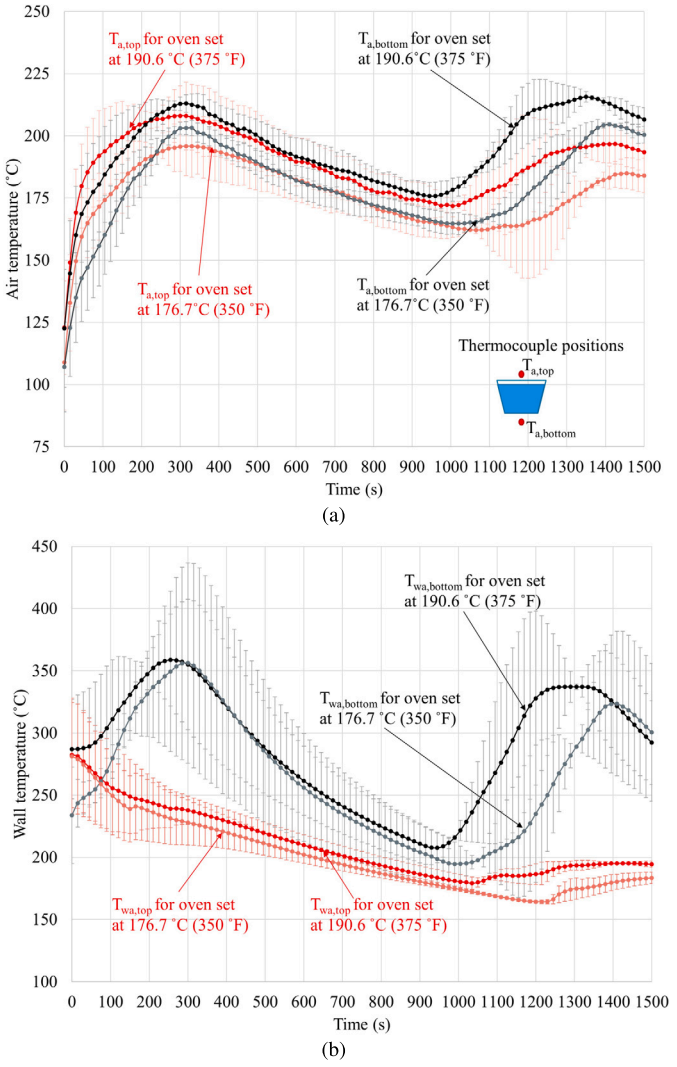

Fig. 11. Measured (a) air and (b) wall temperatures inside the oven above and below the cupcake tray during baking. The error bars indicate variation between experiments.

was provided by an off-the-shelf standard 75 Watt LED bulb (1100 lumen). L^* (lightness), a^* (redness: green to red) and b^* (yellowness: blue to yellow) values of the top surface of the cupcake at different times were measured using the colorimeter. Browning Index ((ΔE)) values were computed from the measured L^*, a^* and b^* values, as shown in Eq. (47). Cake color, expressed as browning, is a critical quality parameter in baking, and hence Browning Index, (ΔE), is chosen as the only variable to study color formation.

5.5. Material properties measurement

The elastic modulus of the batter was measured using a TA Instruments Discovery Hybrid HR-3 type rheometer. One ml of freshly prepared batter was placed between 40 mm parallel plates on the calibrated rheometer, and an oscillatory sheer test of 0.1 Hz with a temperature sweep from 25 °C to 70 °C was conducted to record the elastic moduli. The elastic modulus of the baked cupcake was measured using a TA Instruments DMA Q800 type DMTA (Dynamic Mechanical Thermal Analysis). A 10 mm cubic sample of cake crumbs was cut out from freshly baked cupcakes and placed between clamps on the calibrated DMTA. Compression tests were conducted to record the elastic moduli. Three replicates were carried out, and the average moduli were noted, as shown in Fig. 7a.

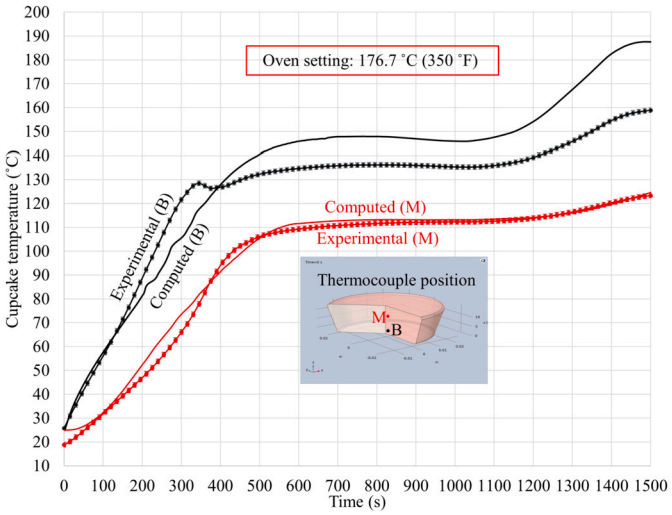

Fig. 12. Cake temperatures at a point close to the center (M) and close to the bottom surface (B) with the oven set at 176.7 °C (350 °F).

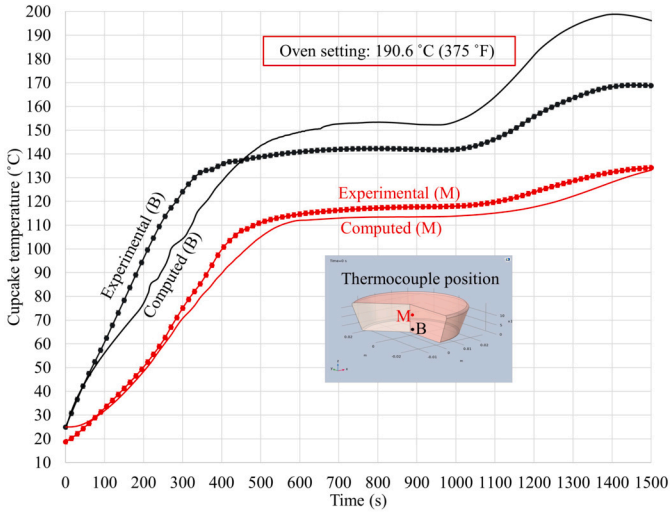

Fig. 13. Cake temperatures at a point close to the center (M) and close to the bottom surface (B) with the oven set at 190.6 °C (375 °F).

6. Results and discussions

The model was validated by experimentally measuring the performance metrics of the cupcake, such as internal temperature, moisture loss, and oven rise during the baking process. Transient changes in the model parameters and their mechanistic effect on the cupcake's surface and internal physical condition through the cooking cycle are discussed next, with validation included in the individual sections.

6.1. Dynamics of the baking process

The computational study gives us deep insights into the dynamics during baking and pinpoints the interplay of physics inside the cupcake at different stages during baking, which cannot be obtained with experiments and simplified models. Temperature, evaporation rate, moisture loss, pressure development, and oven rise are presented in this section, followed by sensitivity analysis.

6.1.1. Spatial temperature profile

Measured and predicted temperatures at two different points inside the cupcake during baking with the oven set at 176.7 °C (350 °F) and 190.6 °C (375 °F) are compared in Fig. 12 and Fig. 13, respectively. Predicted temperatures near the center of the cupcake compare very well with measured temperatures throughout the baking cycle for both oven settings.

At a point close to the bottom surface, the model reasonably predicts the first 200 s of baking for both oven settings but provides higher temperatures for the rest of the baking cycle while still predicting the right trend. The temperature rise inside the cupcake shows three distinct phases, a steady rise during the initial phase, stabilizing during the mid-phase due to large evaporative cooling, and an increase toward the end. In the initial phase, the nearly linear temperature rise means more than conduction heating, with perhaps all three heating modes (conduction, flow, evaporation) active. Fig. 14b later shows that evaporation is significantly present in these early stages for the bottom location. During the mid-phase, since evaporation is always there (see also Fig. 14b), temperature values must be moderated by the latent heat of evaporation. Almost a pseudo-steady state is reached where the bottom temperature stays higher than the midpoint temperature. The temperature increase toward the end is primarily due to the increase in the wall and air temperatures in the oven, which drives the baking process (Fig. 11a, Fig. 11b). Although there has been significant moisture loss, substantial moisture is still left to make this temperature increase near the end unlikely due to lack of evaporation. When the model was run (data not shown) for very long times (2500 s with no cycling of the oven temperature), the cake temperatures did not go up in the third stage since, even at these long times, there was significant moisture left in it. Previous attempts at modeling cupcake baking have found it challenging to match temperatures during different stages of baking (Sakin et al., 2007), perhaps due to the complexity of the baking process during the initial stages (Section 6.1).

Temperatures inside the cupcake (Fig. 14a) begin to rise from outside to inside, evaporating water (Fig. 14b) in the batter and causing subsequent moisture loss from the top surface of the cupcake (Fig. 17a) (discussed later). Temperatures do not rise as much within the cupcake due to a combination of large evaporative cooling and an increase in the thermal resistance of the outer region (where water is replaced by the lower thermal conductivity vapor and carbon dioxide), slowing heat transfer to the center. Sakin et al. (2007) also show the center temperatures not rising much for hours of baking.

6.1.2. Rate of evaporation

Evaporation (Fig. 14b) progresses from the outside to the inside with a sharp front (evaporation front) where vapor generation occurs. The pressure developed due to evaporation pushes the generated hot vapor towards the colder center of the cupcake, which condenses to water with a sharp front (condensation front) marked in Fig. 14b. Initially, the evaporation rate is higher due to a large temperature gradient near the surface, causing a very high heat transfer rate. But, as the cupcake batter rises, the evaporation rate reduces due to decreased heat transfer rate.

Since the region outside the evaporation front, i.e., between the evaporation front and the outer boundary (Fig. 14b) primarily consists of vapor and carbon dioxide, its effective thermal conductivity is small, reducing heat transfer to the core and maintaining lower temperatures at the center. Evaporation and the condensation front move inward and up during baking due to inward heat transfer and upward material deformation. This creates more regions of primarily gas between the bottom surface of the cupcake and the evaporation front, thus slowing down heat transfer and moisture loss from the center, explaining why the center temperatures do not rise much for hours of baking as reported in previous experiments (Sakin et al., 2007).

6.1.3. Moisture loss

Moisture loss in the cupcake during baking with the oven set at 176.7 °C (350 °F) and 190.6 °C (375 °F) (Fig. 15, Fig. 16) show excellent agreement between model prediction and experiments. The moisture loss for the 190.6 °C (375 °F) setting is higher than the 176.7 °C

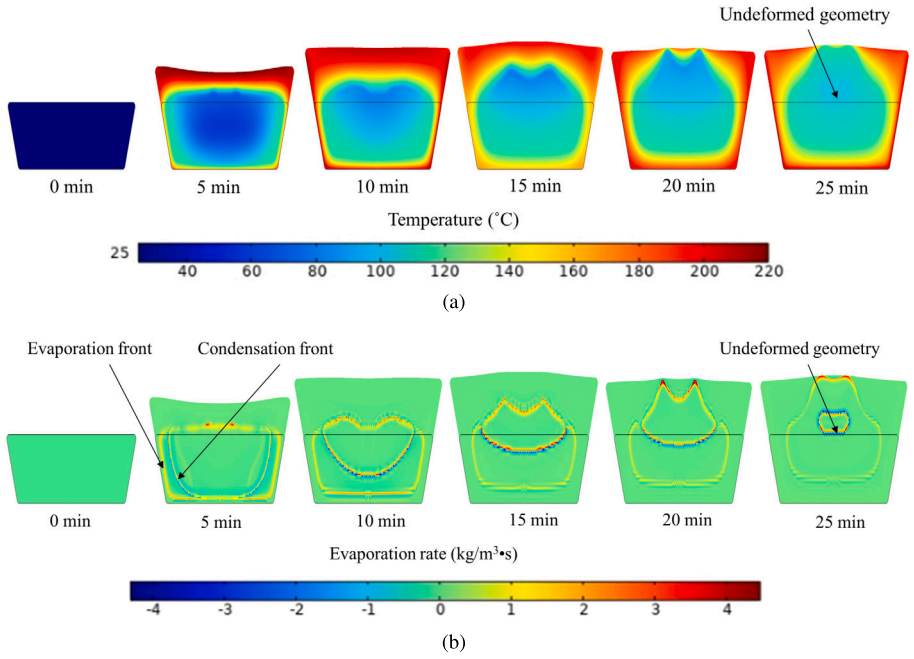

Fig. 14. (a) Temperature and (b) evaporation rate profiles inside the cupcake during baking.

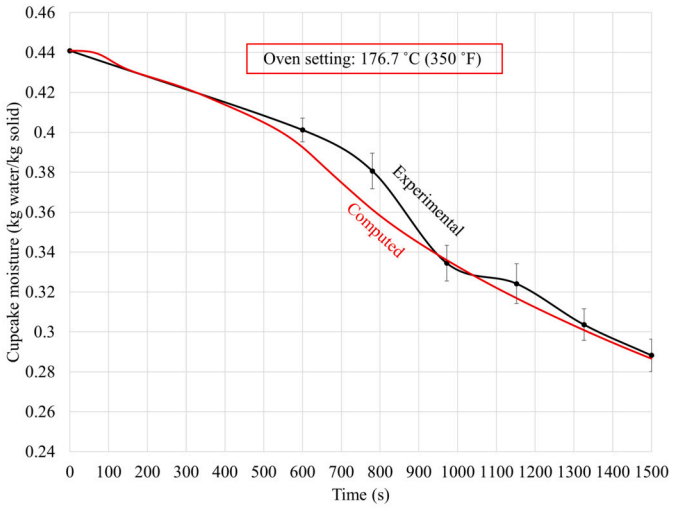

Fig. 15. Moisture content of the cupcake during baking with the oven set at 176.7 °C (350 °F).

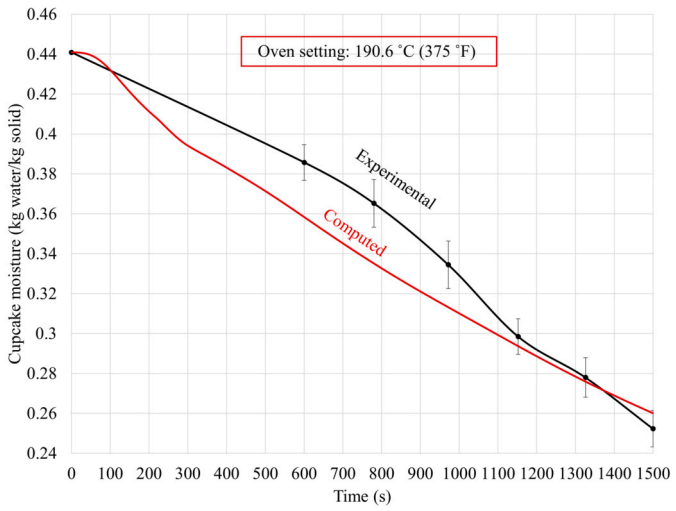

Fig. 16. Moisture content of the cupcake during baking with the oven set at 190.6 °C (375 °F).

(350 °F) setting. The effect of the oven's cyclic air and wall temperatures that drive the process is not clearly seen in the evolution of moisture loss.

Computed liquid water saturation and vapor mass fraction inside the cupcake at different times during baking are shown in Fig. 17a and 17b, respectively. As the evaporation front moves towards the center (Fig. 14b), the generated water vapor at the evaporation front moves outward and inward. Vapor generated close to the bottom, and the lateral sides push the evaporation front and the water content in the batter towards the center and find a way to the top as it cannot leave through the bottom and the lateral surfaces. The pressure developed inside the batter (Fig. 20b) drives the generated vapor toward the cold center, condensing it inside the batter's red regions (Fig. 17a). Vapor moving outward leaves through the top surface.

6.1.4. Vapor and CO_2 generation and pressure development

Vapor and gas (vapor+CO_2) pressure development inside the cupcake during baking is shown in Fig. 20a and 20b, respectively. Vapor generated (shown as absolute pressure) close to the bottom, and the lateral sides encounter more resistance (greater distance to cover), leading to higher pressure. As the batter transforms with heat to a less permeable solid foam (Fig. 21a), higher pressure regions appear due to trapped gas, as shown as an increase in the gas pressure (Fig. 20b). The velocity field (Fig. 20b and 21a) shows that the gases (vapor and the carbon dioxide) and the liquid water in the batter are pushed toward the more permeable central regions as the batter becomes a less permeable solid foam on the outside. The gas pressure inside the cupcake expressed in gauge pressure shows the pressure development that drives the deformation.

6.1.5. Oven rise

The measured and predicted oven rise (height change) of the cupcake during baking compares well, as shown in Fig. 18 and Fig. 19, respectively. For the 176.7 °C (350 °F) oven setting, the model predicts no oven rise during the first 150 s, a massive oven rise (over 100%) between 150 s and 850 s, and a continuous shrinkage (around 10%)

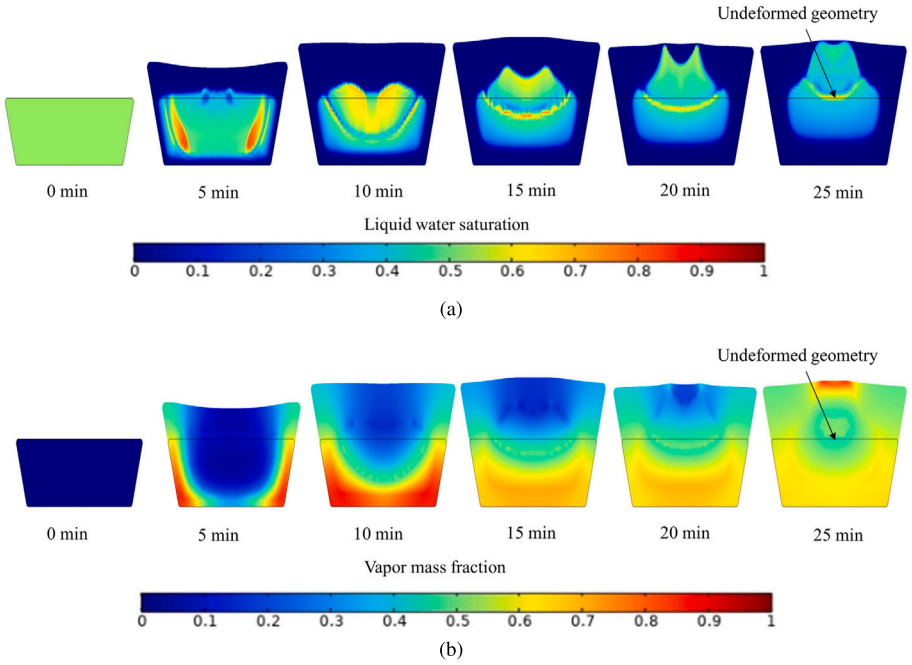

Fig. 17. (a) Liquid water saturation inside the cupcake during baking - the red regions show the effects of condensation. (b) Vapor mass fraction inside the cupcake during baking.

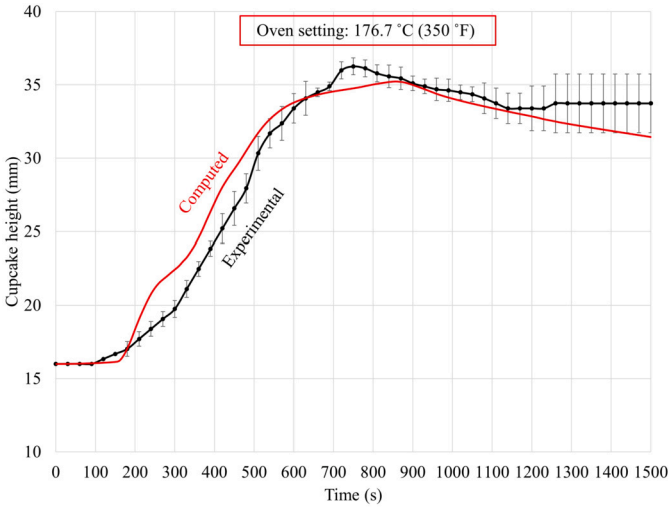

Fig. 18. Oven rise of the cupcake during baking with the oven set at 176.7 °C (350 °F).

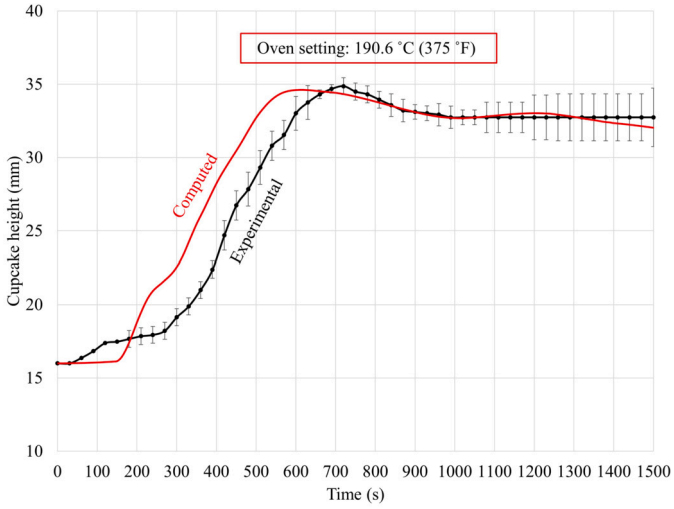

Fig. 19. Oven rise of the cupcake during baking with the oven set at 190.6 °C (375 °F).

during the rest of the baking cycle. For the 190.6 °C (375 °F) setting, the model predicts no oven rise during the first 150 s, a massive oven rise (over 100%) between 150 s and 600 s, and a continuous shrinkage (around 10%) during the rest of the baking cycle. The model follows experimental results in predicting a faster oven rise to peak height for the 190.6 °C (375 °F) setting. The significant variation in oven rise during different stages of baking is primarily due to changes in mechanical properties of the batter during which the aqueous, fluid batter rises to form a foam-like structure as discussed in Section 6.1.5. Measured oven rise shows significant variations in carefully repeated experiments, representing the complex nature of the process. The effect of the oven's cyclic air and wall temperatures that drive the process is not clear in the evolution of cake height.

The evolution of gas pressure inside the batter and the transformation of the cupcake batter to a less permeable solid foam combine to cause the oven rise and top surface shape (Fig. 20a, 20b and 21a). It is seen from the intermediate shape profiles that the shape of the cupcake's top surface (Fig. 22) is a direct result of gas pressure evolution inside the batter (Fig. 20b). Initially (at around 10 min), the higher pressure near the periphery pushes the batter up higher than at the center (Fig. 20b). Later, the material transforms into a less permeable solid with higher pressure in the central region leading to a dome shape. This shape is permanent as the material transformation is complete (around 22 min), with the entire batter becoming a solid foam. The peak oven rise reduces during the final stages of baking to 30% at the perimeter and about 10% at the center. This phenomenon must be associated with the formation of solid foam with a higher material modulus, as is clear from Figs. 20a, 20b and 21a. The evolution of elastic modulus with time (Fig. 21b) from 20 Pa, characterizing the elastic nature of the aqueous batter, to 2000 Pa, characterizing the set cake, follows the evolution of permeability (Fig. 21a), as both the transformations are temperature dependent and occur during the starch gelatinization range of temperatures.

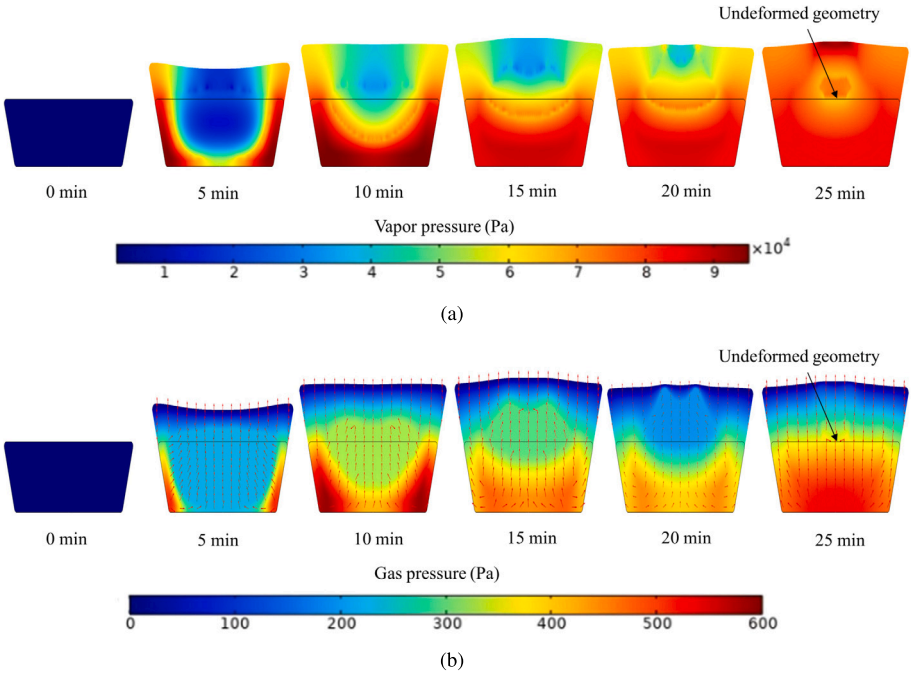

Fig. 20. (a) Vapor pressure (absolute pressure) (b) gas pressure (gauge pressure) inside the cupcake during baking.

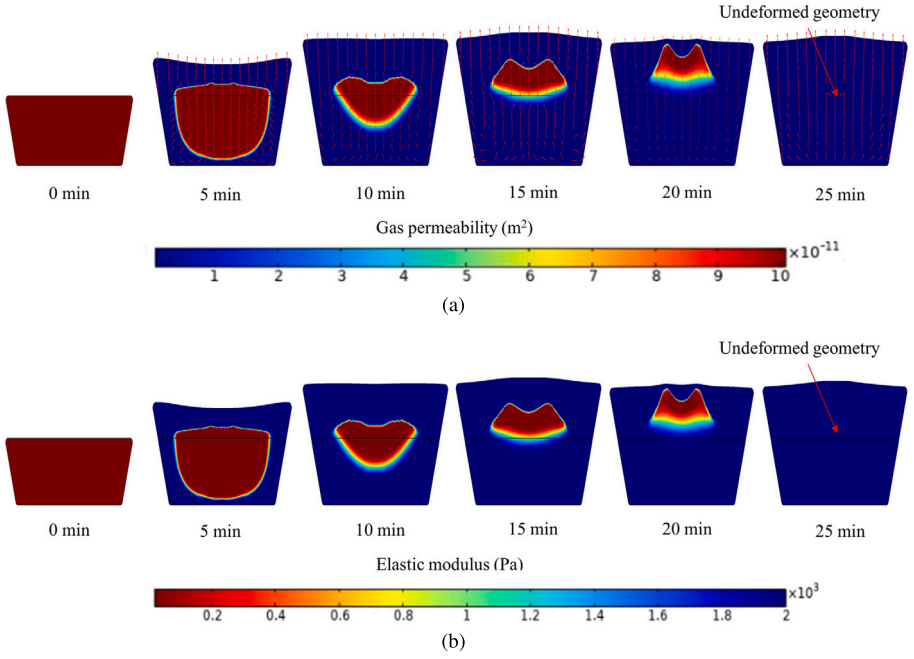

Fig. 21. (a) gas permeability (b) elastic modulus inside the cupcake during baking.

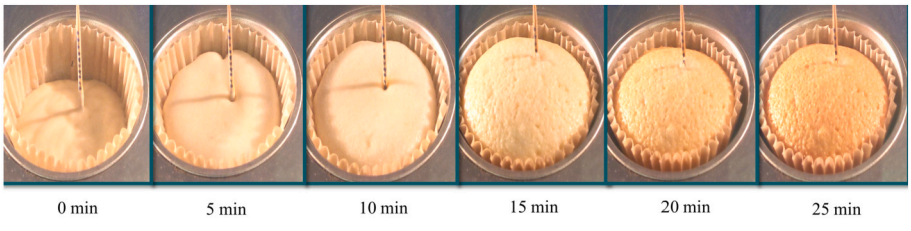

Fig. 22. Shape change of the cupcake during baking at different times.

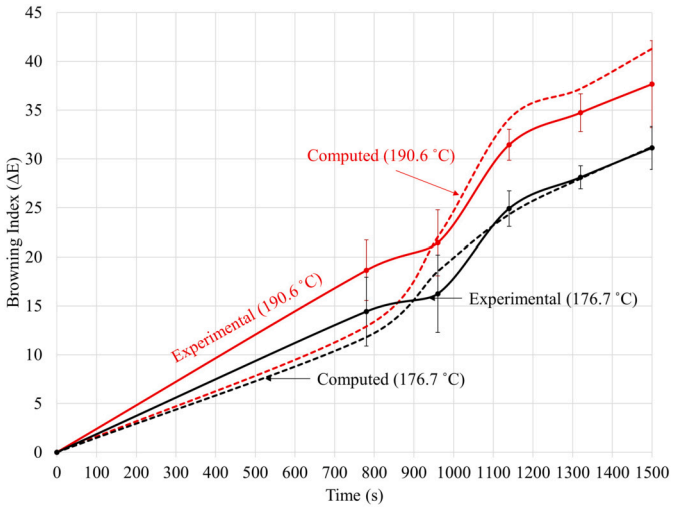

Fig. 23. Surface browning of the cupcake during baking in the oven set at 176.7 °C (350 °F) and 190.6 °C (375 °F).

6.1.6. Surface browning

Browning of the cupcake surface during baking (Fig. 23) shows good agreement between the model predictions and experimental data. The parameters for color model (Eq. (48)) are obtained by fitting the predicted color development to an experimental data set of surface browning for the 176.7 °C (350 °F) setting. There is no significant browning till about 16 minutes of baking (Fig. 24), which could explain the considerable variation in the experimental data till this time during the baking process. The oven temperature significantly influences browning development.

6.2. Cupcake baking: a mechanistic understanding

Fig. 25 shows a schematic of the mechanistic sequence of events in a cupcake baking. The process begins by heating liquid batter inside a cooking oven, generating water vapor from evaporation and carbon dioxide from reacting baking powder. Vapor and carbon dioxide leave the cupcake at the surface by diffusion through pore spaces. The cake batter then undergoes a material transformation to a less permeable solid foam at the starch gelatinization temperature trapping the generated gas and causing internal pressure to increase. The increased pressure in the cake material leads to pressure-driven transport of water, vapor and carbon dioxide, and deformation. The geometry sets when the material transformation is complete but shrinks slightly with continued moisture loss.

6.3. Sensitivity analysis

The comprehensive mechanistic model and carefully repeated experimental measurements capture the physics of cake baking well, despite the unavailability of readily usable model parameters, as seen from the results presented. Sensitivity analyses were carried out for two important properties, water activity and elastic modulus, perhaps with the greatest uncertainty.

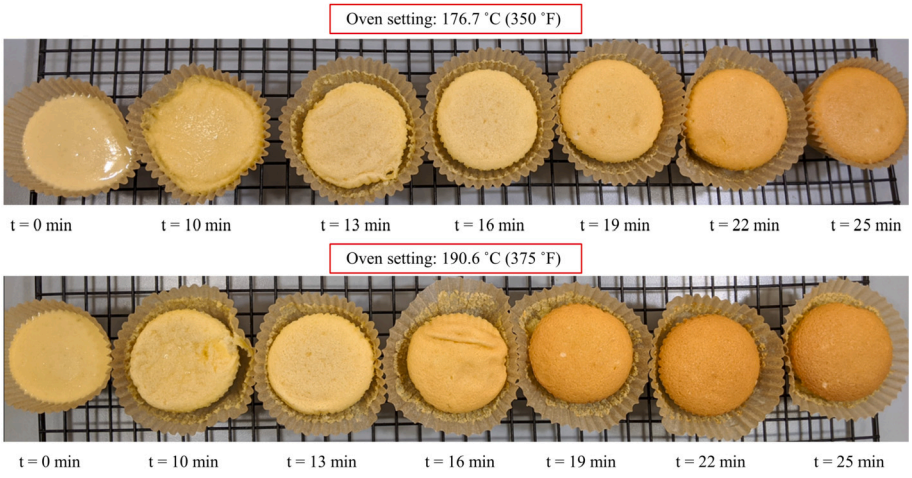

Fig. 24. Surface browning of the cupcake during baking in the oven set at 176.7 °C (350 °F) and 190.6 °C (375 °F).

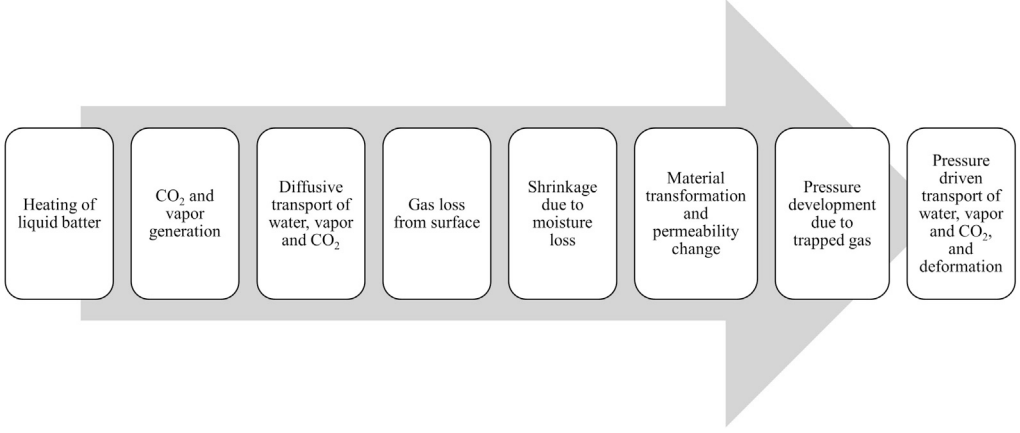

Fig. 25. Schematic showing the sequence of mechanistic events in a cupcake baking.

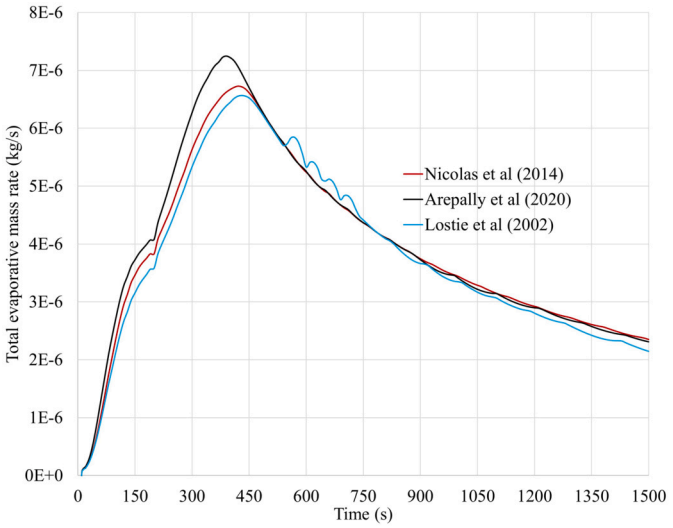

Fig. 26. Sensitivity of the rate of total mass evaporated during baking to three water activity models (Nicolas et al., 2014; Arepally et al., 2020; Lostie et al., 2002).

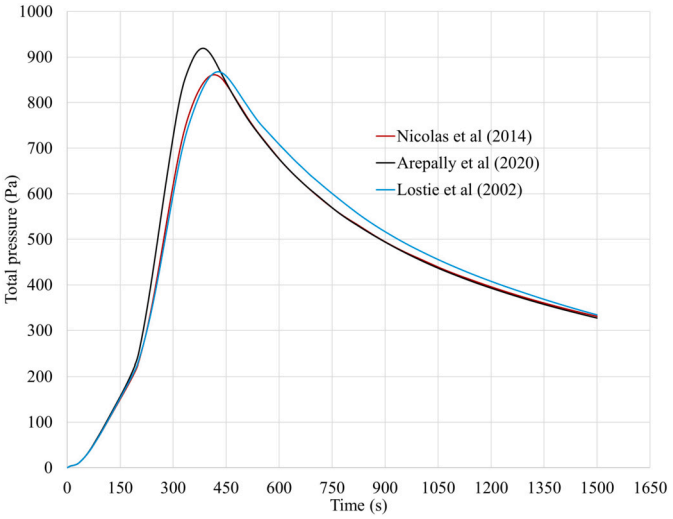

Fig. 27. Sensitivity of the total pressure during baking to three water activity models (Nicolas et al., 2014; Arepally et al., 2020; Lostie et al., 2002).

6.3.1. *Water activity*

The evolution of the total mass of vapor generation and the gas pressure developed inside the batter for three different water activity models is shown in Fig. 26 and Fig. 27, respectively, showing that the effect of the three different water activities on the vapor generation and the subsequent pressure development is insignificant. Thus, the water activities used here are reasonable.

6.3.2. *Elastic modulus*

Fig. 29 shows oven rise during baking computed using two different temperature evolutions (Fig. 28), each approximately defining the lower and upper limits of the measured values. Thus, computed oven rise is relatively insensitive to the upper and lower limits of material moduli, making the choice of elastic modulus reasonable.

7. Conclusions

A mechanistic model for cupcake baking was developed that includes coupled multiphase heat and mass transport, large deformation and large changes in mechanical properties. The model was validated

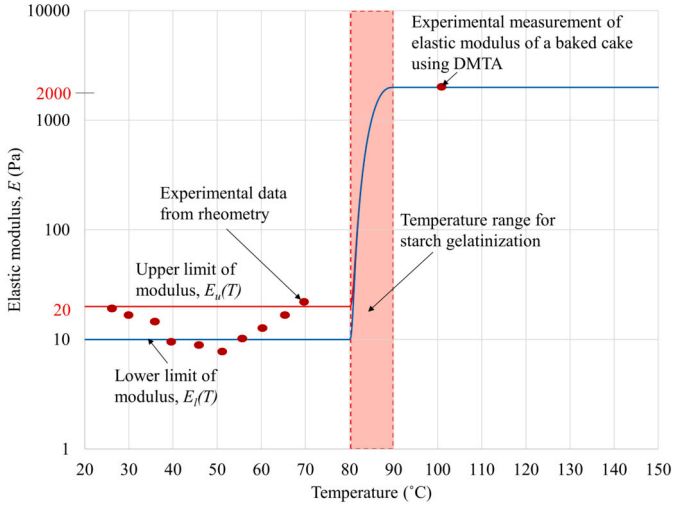

Fig. 28. Variation in elastic modulus of the batter with temperature.

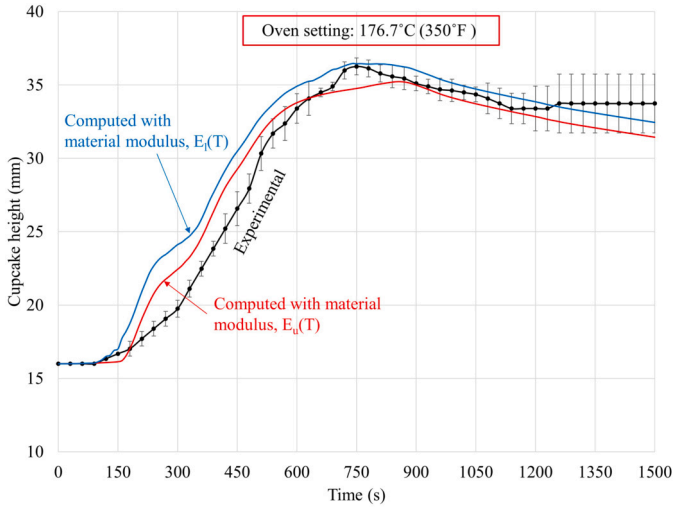

Fig. 29. Sensitivity of the cupcake height during baking to variation in elastic modulus of the batter.

by experimentally measured metrics such as oven rise, color, weight loss, and internal temperatures for different oven settings during the baking cycle. Key parameters for the baking process were identified, and sensitivity analyses were performed. The model enabled a comprehensive quantitative understanding of the effect of coupled transport and deformation on the surface and internal physical conditions. Being first principle-based and comprehensive, the model can easily be extended to understand the role of ingredients on the critical performance metrics of cupcake and other baked goods (Seranthian, 2023). The model can also study the interaction between food and oven physics when coupled with a mechanistic model for a cooking oven providing the convective and radiative fluxes (Seranthian, 2023). As part of computer-aided food engineering (Datta et al., 2022), it will significantly enhance the optimization of equipment (oven) and baked product design. While the mechanistic model-based computations here are resource intensive, data-driven surrogate models trained by the simulation results from this model can make computing resource a non-issue (Ghosh and Datta, 2023).

Key conclusions from this work are: (1) the model accurately predicts the cupcake's internal temperatures, moisture loss, deformation, and color formation during baking for different oven settings; (2) large evaporative cooling inside the cupcake muffles the effect of variation in oven temperatures; (3) there are significant variations in oven rise

during different stages of baking due to large changes in mechanical properties during the process; (4) there is no significant browning till about 16 minutes of baking; (5) temperatures only rise a little within the cupcake due to ample evaporative cooling and increased thermal resistance of the outer regions; (6) a sharp evaporation front accompanies vapor generation; (7) the vapor generated close to the bottom and lateral sides move toward the highly permeable colder center regions causing condensation; (8) high-pressure regions appear in the batter only after the batter transforms with heat to a less permeable solid foam; and (9) the oven rise profile during baking follows the pressure profile inside the batter until the material is set.

Nomenclature

Symbol	Description	Units
c	concentration	kg/m^3
C_p	specific heat capacity	J/kg K
C_g	molar density	kmol/m^3
$D_{eff,g}$	vapor diffusivity in air	m^2/s
$D_{w,cap}$	capillary diffusivity	m^2/s
E	elastic modulus	N/m^2
$\mathbf{E}$	Green-Lagrange strain tensor	
$\mathbf{F}$	deformation tensor	
h_t	heat transfer coefficient	W/m^2 K
h_m	mass transfer coefficient	m/s
$\dot{I}$	rate of evaporation	kg/m^3 s
$\mathbf{I}$	Identity tensor	
J	Jacobian	
k_{in}	intrinsic permeability	m^2
k_r	relative permeability	
K_{evap}	evaporation rate constant	1/s
m	overall mass fraction	
M	moisture content (dry basis)	kg water/kg dry solid
M	molecular weight	kg
$\vec{n}$	mass flux	kg/m^2 s
$\vec{N}$	unit normal	
p	pressure	Pa
r	radius	m
S_i	saturation of fluid phase i	
$\mathbf{S}$	Piola–Kirchoff stress tensor	Pa
t	time	s
T	temperature	°C
$\vec{u}$	displacement	m
$\vec{v}$	velocity	m/s
x_i	mole fraction of component i in gas phase	
V	volume	m^3
Greek symbols		
ρ	density	kg/m^3
λ	latent heat of vaporization	J/kg
ω_i	mass fraction of component i	
ϕ	porosity	
σ	stress	Pa
ε	strain	
Subscripts		
amb	ambient	
a	air	
cap	capillary	
eff	effective	
f	fluid	
G	ground (stationary observer)	
g	gas	
i	ith phase	
M	moisture	
s	solid	
sat	saturated	
$surf$	surface	
v	vapor	
w	water	
wa	wall	
0	at time $t = 0$	

Declaration of competing interest

The authors declare the following financial interests/personal relationships, which may be considered as potential competing interests: Kalayarasan Seranthian reports financial support was provided by Whirlpool Corp.

Data availability

The authors do not have permission to share data.

Acknowledgements

This work was carried out with partial financial support from Whirlpool Corporation. The authors wish to thank their industrial collaborators, Shaoping Shi, Lucas Baldani, Amit Khanchi, Christopher Stuart, and Nicholas Kormanik. This work used the Cornell Center for Materials Research Shared Facilities, which are supported through the NSF MRSEC program (DMR-1719875).

References

Andrade, R.D., Lemus, R., Perez, C.E., 2011. Models of sorption isotherms for food: uses and limitations. Vitae 18 (3), 325–334.
Antoine, M., 1888. Nouvelle relation entre les tensions et les temperatures. C. R. Held Seanc. Acad. Sci. Paris 107, 681–684.
Aregawi, W.A., Defraeye, T., Verboven, P., Herremans, E., De Roeck, G., Nicolai, B., 2013. Modeling of coupled water transport and large deformation during dehydration of apple tissue. Food Bioprocess Technol. 6 (8), 1963–1978.
Arepally, D., Reddy, R.S., Goswami, T.K., Datta, A.K., 2020. Biscuit baking: a review. Lebensm.-Wiss. Technol. 131, 109726.
Bassal, A., Vasseur, J., Loncin, M., 1993. Sorption isotherms of food materials above 100 °C. Lebensm.-Wiss. Technol. 26 (6), 505–511.
Basu, S., Shivhare, U., Mujumdar, A., 2006. Models for sorption isotherms for foods: a review. Dry. Technol. 24 (8), 917–930.
Bear, J., 1988. Dynamics of Fluids in Porous Media. Courier Corporation.
Bennion, E.B., Bamford, G., 1997. The Technology of Cake Making. Springer Science & Business Media.
Book, S., Brill, R., et al., 2015. Effects of chemical leavening on yellow cake properties. Cereal Foods World 60 (2), 71–75.
Brodie, J., Godber, J., 2000. Bakery processes, chemical leavening agents. In: Kirk-Othmer Encyclopedia of Chemical Technology.
Cevoli, C., Panarese, V., Catalogne, C., Fabbri, A., 2020. Estimation of the effective moisture diffusivity in cake baking by the inversion of a finite element model. J. Food Eng. 270, 109769.
Choi, Y., Okos, M., 1986. Thermal Properties of Liquid Foods.
Daniels, D.G., Fisher, N., 1976. Release of carbon dioxide from dough during baking. J. Sci. Food Agric. 27 (4), 351–357.
Datta, A., 2007. Porous media approaches to studying simultaneous heat and mass transfer in food processes. i: Problem formulations. J. Food Eng. 80 (1), 80–95.
Datta, A., Nicolaï, B., Vitrac, O., Verboven, P., Erdogdu, F., Marra, F., Sarghini, F., 2022. Computer-aided food engineering. Nat. Food, 1–11.
Dhall, A., Datta, A.K., 2011. Transport in deformable food materials: a poromechanics approach. Chem. Eng. Sci. 66 (24), 6482–6497.
Epaarachchi, J., 2011. The effect of viscoelasticity on fatigue behaviour of polymer matrix composites. In: Creep and Fatigue in Polymer Matrix Composites. Elsevier, pp. 492–513.
Fennema, O.R., 1996. Food Chemistry, vol. 76. CRC Press.
Feyissa, A.H., Gernaey, K., Ashokkumar, S., Adler-Nissen, J., 2011. Modelling of coupled heat and mass transfer during a contact baking process. J. Food Eng. 106 (3), 228–235.
Foot, F.N., 1906. Baking Powder and Other Leavening Agents. Spice Mill Publishing Company.
Ghosh, D., Datta, A., 2023. Deep learning enabled surrogate model of complex food processes for rapid prediction. Chem. Eng. Sci. 270, 118515.
Godefroidt, T., Ooms, N., Pareyt, B., Brijs, K., Delcour, J.A., 2019. Ingredient functionality during foam-type cake making: a review. Compr. Rev. Food Sci. Food Saf. 18 (5), 1550–1562.
Gulati, T., Datta, A.K., 2016. Coupled multiphase transport, large deformation and phase transition during rice puffing. Chem. Eng. Sci. 139, 75–98.
Guy, R.C., Sahi, S.S., 2006. Application of a lipase in cake manufacture. J. Sci. Food Agric. 86 (11), 1679–1687.
Hajikarimi, P., Nejad, F.M., 2021. Applications of Viscoelasticity: Bituminous Materials Characterization and Modeling. Elsevier.
Halder, A., Dhall, A., Datta, A., 2007. An improved, easily implementable, porous media based model for deep-fat frying: Part i: Model development and input parameters. Food Bioprod. Process. 85 (3), 209–219.
Incropera, F., DeWitt, D., 1985. Introduction to Heat Transfer.
Jacob, H.E., 2007. Six Thousand Years of Bread: Its Holy and Unholy History. Skyhorse Publishing Inc.

Le, C., Ly, N., Postle, R., 1995. Heat and mass transfer in the condensing flow of steam through an absorbing fibrous medium. Int. J. Heat Mass Transf. 38 (1), 81–89.
Lewis, M.J., 1990. Physical Properties of Foods and Food Processing Systems. Elsevier.
Lostie, M., Peczalski, R., Andrieu, J., Laurent, M., 2002. Study of sponge cake batter baking process. ii. Modeling and parameter estimation. J. Food Eng. 55 (4), 349–357.
Lostie, M., Peczalski, R., Andrieu, J., 2004. Lumped model for sponge cake baking during the “crust and crumb” period. J. Food Eng. 65 (2), 281–286.
Martins, S.I., Jongen, W.M., Van Boekel, M.A., 2000. A review of Maillard reaction in food and implications to kinetic modelling. Trends Food Sci. Technol. 11 (9–10), 364–373.
McCabe, W.L., Smith, J.C., Harriott, P., 1993. Unit Operations of Chemical Engineering, vol. 5. McGraw-Hill, New York.
Miller, R., 2016. Leavening agents. In: Caballero, B., Finglas, P.M., Toldrá, F. (Eds.), Encyclopedia of Food and Health. Academic Press, Oxford. ISBN 978-0-12-384953-3, pp. 523–528.
Mizukoshi, M., 1985. Model studies of cake baking. v. Cake shrinkage and shear modulus of cake batter during baking. Cereal Chem. (USA).
Mizukoshi, M., Kawada, T., Matsui, N., 1979. Model studies of cake baking. i. Continuous observations of starch gelatinization and protein coagulation during baking. Cereal Chem.
Mizukoshi, M., Maeda, H., Amano, H., 1980. Model studies of cake baking. ii. Expansion and heat set of cake batter during baking. Cereal Chem. (USA).
Moldrup, P., Olesen, T., Yoshikawa, S., Komatsu, T., McDonald, A.M., Rolston, D.E., 2005. Predictive-descriptive models for gas and solute diffusion coefficients in variably saturated porous media coupled to pore-size distribution: iii. Inactive pore space interpretations of gas diffusivity. Soil Sci. 170 (11), 867–880.
Nicolas, V., Salagnac, P., Glouannec, P., Ploteau, J.-P., Jury, V., Boillereaux, L., 2014. Modelling heat and mass transfer in deformable porous media: application to bread baking. J. Food Eng. 130, 23–35.
Nicolas, V., Vanin, F., Grenier, D., Lucas, T., Doursat, C., Flick, D., 2016. Modeling bread baking with focus on overall deformation and local porosity evolution. AIChE J. 62 (11), 3847–3863.
Purlis, E., Salvadori, V.O., 2009. Modelling the browning of bread during baking. Food Res. Int. 42 (7), 865–870.
Pyler, E., Gorton, L., 2008. Baking Science & Technology: Volume I: Fundamentals & Ingredients. Sosland Pub.
Rubinstein, M., Colby, R.H., et al., 2003. Polymer Physics, vol. 23. Oxford University Press, New York.
Sablani, S., Marcotte, M., Baik, O., Castaigne, F., 1998. Modeling of simultaneous heat and water transport in the baking process. Lebensm.-Wiss. Technol. 31 (3), 201–209.
Sakin, M., Kaymak-Ertekin, F., Ilicali, C., 2007. Simultaneous heat and mass transfer simulation applied to convective oven cup cake baking. J. Food Eng. 83 (3), 463–474.
Sakin, M., Kaymak-Ertekin, F., Ilicali, C., 2009. Convection and radiation combined surface heat transfer coefficient in baking ovens. J. Food Eng. 94 (3–4), 344–349.
Sakin-Yilmazer, M., Kaymak-Ertekin, F., Ilicali, C., 2012. Modeling of simultaneous heat and mass transfer during convective oven ring cake baking. J. Food Eng. 111 (2), 289–298.
Scarpa, F., Milano, G., 2002. The role of adsorption and phase change phenomena in the thermophysical characterization of moist porous materials. Int. J. Thermophys. 23 (4), 1033–1046.
Schwartzberg, H.G., Wu, J.P., Nussinovitch, A., Mugerwa, J., 1995. Modelling deformation and flow during vapor-induced puffing. J. Food Eng. 25 (3), 329–372.
Seranthian, K., 2023. Multimode heat transfer in a cooking oven with multiphase transport, poromechanics, and material transformation in food. PhD thesis. Cornell University.
Sumnu, S.G., Sahin, S., 2008. Food Engineering Aspects of Baking Sweet Goods. CRC Press.
Tanaka, F., 2011. Polymer Physics: Applications to Molecular Association and Thermoreversible Gelation. Cambridge University Press.
Tanikawa, W., Shimamoto, T., 2009. Comparison of Klinkenberg-corrected gas permeability and water permeability in sedimentary rocks. Int. J. Rock Mech. Min. Sci. 46 (2), 229–238.
Ureta, M.M., Olivera, D.F., Salvadori, V.O., 2016. Baking of sponge cake: experimental characterization and mathematical modelling. Food Bioprocess Technol. 9 (4), 664–674.
Ureta, M.M., Olivera, D.F., Salvadori, V.O., 2017. Influence of baking conditions on the quality attributes of sponge cake. Food Sci. Technol. Int. 23 (2), 156–165.
van der Lijn, J., 1976. Simulation of Heat and Mass Transfer in Spray Drying. Wageningen University and Research.
Vujošević, L., Lubarda, V., 2002. Finite-strain thermoelasticity based on multiplicative decomposition of deformation gradient. Theor. Appl. Mech. 28–29, 379–399.
Warning, A., Verboven, P., Nicolaï, B., van Dalen, G., 2014. Computation of mass transport properties of apple and rice from x-ray microtomography images. Innov. Food Sci. Emerg. Technol. 24, 14–27.
Zanoni, B., Peri, C., Bruno, D., 1995. Modelling of browning kinetics of bread crust during baking. Lebensm.-Wiss. Technol. 28 (6), 604–609.
Zhang, J., Datta, A., 2006. Mathematical modeling of bread baking process. J. Food Eng. 75 (1), 78–89.